AA

DEPARTMENT OF HEALTH AND HUMAN SERVICES	LEAVE BLANK FOR PHS USE ONLY.		
PUBLIC HEALTH SERVICE	Type	Activity	Number
· GRANT APPLICATION	Review Group		Formerly
Follow instructions carefully. Type in the unshaded areas only.	Council/Board (Month, Year)		Date Received

1. TITLE OF PROJECT (Do not exceed 56 typewriter spaces.)

Quantitative Inverse Electrocardiography

2. RESPONSE TO SPECIFIC PROGRAM ANNOUNCEMENT ☐ NO ☒ YES (If "YES," state RFA number and/or announcement title)

Number: **R29** Title: **FIRST**

3. PRINCIPAL INVESTIGATOR/PROGRAM DIRECTOR   ☒ NEW INVESTIGATOR

3a. NAME (Last, first, middle)	3b. DEGREE(S)	3c. SOCIAL SECURITY NO.
Johnson, Christopher R.	**PhD**	**499-68-3733**

3d. POSITION TITLE

Research Asst Professor of Medicine

3f. DEPARTMENT, SERVICE, LABORATORY, OR EQUIVALENT

Nora Eccles Harrison CVRTI

3g. MAJOR SUBDIVISION

School of Medicine

3h. TELEPHONE (Area code, number, and extension)

(801) 581-8183

3e. MAILING ADDRESS (Street, city, state, zip code)

University of Utah
Nora Eccles Harrison CVRTI
Bldg 500
Salt Lake City, Utah 84112

4. HUMAN SUBJECTS		IRB approval date	4b. Assurance of compliance no.	5 VERTEBRATE ANIMALS		IACUC approval date	5b. Animal welfare assurance no.
☐ 4a. NO ☒ YES	If "YES," exemption no. or	**10/17/90**	**M 1082**	☐ 5a. NO ☒ YES	If "YES."	**9/27/88**	**A3031-01**

6. DATES OF ENTIRE PROPOSED PROJECT PERIOD		7. COSTS REQUESTED FOR FIRST 12-MONTH BUDGET PERIOD		8. COSTS REQUESTED FOR ENTIRE PROPOSED PROJECT PERIOD	
From (YYMMDD)	Through (YYMMDD)	7a. Direct Costs	7b. Total Costs	8a. Direct Costs	8b. Total Costs
91-12-01	**96-11-30**	**$ 77,338**	**$ 97,154**	**$ 350,000**	**$ 502,057**

9. PERFORMANCE SITES (Organizations and addresses)

University of Utah
Nora Eccles Harrison Cardiovascular
 Research & Training Institute
Building 500
Salt Lake City, Utah 84112

10. INVENTIONS (Competing continuation application only)

☐ NO ☐ YES If "YES." ☐ Previously reported ☐ Not previously reported

11. NAME OF APPLICANT ORGANIZATION

University of Utah
ADDRESS (Street, city, state, and zip code)

Room 309 Park Building
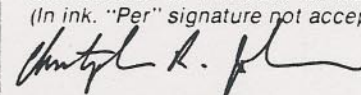**University of Utah**
Salt Lake City, Utah 84112

13. ENTITY IDENTIFICATION NUMBER	Congressional District
1876000525 A1	**2nd**

12. TYPE OF ORGANIZATON

☒ Public: Specify ☐ Federal ☒ State ☐ Local
☐ Private Nonprofit **University**
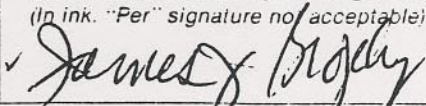☐ For Profit (General) ☐ For Profit (Small Business)

14. ORGANIZATIONAL COMPONENT TO RECEIVE CREDIT TOWARDS A BIOMEDICAL RESEARCH SUPPORT GRANT

Code: **01** Identification: **School of Medicine**

15. NAME OF OFFICIAL IN BUSINESS OFFICE

Robert G. Glass
TELEPHONE (Area code, number, and extension)

(801) 581-6903
TITLE

Director, Office of Sponsored Projects
ADDRESS

Room 309 Park Building
University of Utah
Salt Lake City, Utah 84112

16. NAME OF OFFICIAL SIGNING FOR APPLICANT ORGANIZATION

James J. Brophy or Ronald J. Pugmire
TELEPHONE (Area code, number, and extension)

(801) 581-7236
TITLE

VP for Research or Assoc VP for Research
ADDRESS

Room 210 Park Building
Salt Lake City, Utah 84112

17. PRINCIPAL INVESTIGATOR/PROGRAM DIRECTOR ASSURANCE: I agree to accept responsibility for the scientific conduct of the project and to provide the required progress reports if a grant is awarded as a result of this application. Willful provision of false information is a criminal offense (U.S. Code, Title 18, Section 1001).	SIGNATURE OF PERSON NAMED IN 3a (In ink. "Per" signature not acceptable.) *[signature]*	DATE **25 January 1991**
18. CERTIFICATION AND ACCEPTANCE: I certify that the statements herein are true and complete to the best of my knowledge, and accept the obligation to comply with Public Health Service terms and conditions if a grant is awarded as the result of this application. A willfully false certification is a criminal offense (U.S. Code, Title 18, Section 1001).	SIGNATURE OF PERSON NAMED IN 16 (In ink. "Per" signature not acceptable) ✓ *[signature]*	DATE **JAN 29 1991**

PHS 398 (Rev. 10/88)   AA

No U 2472

llccir 9-8-80

UNIVERSITY OF UTAH LABORATORY ANIMAL PROTOCOL
(Please Type)

I. Name of Princ. Invest. Taccardi, Bruno	Title Visiting Prof of Med	Department CVRTI	Phone 581-8183
Name of Co-Invest. Watabe, Shinji	Title Research Associate	Department CVRTI	Phone 581-8183
Lab Contact Jayne Davis (Ext 8183)		Emergency Phone No. (P.I.'s Home) 583-4081	

II. Title of Project __THREE-DIMENSIONAL MAPPING OF CARDIAC ELECTRIC FIELDS__

Type of Project   ☒ Research   ☐ Educ. & Training   ☐ Other (explain)

Expected starting date __10/1/88__   Expected completion date __9/30/91__

III. Primary Source of Funding __Treadwell Foundation__   Account No. __6-47467__   Grant No. __None__

Title of Grant ___"Three-dimensional Mapping of the Cardiac Electric Field"___

Status   ☐ New   ☐ Competing Renewal   ☒ Continuation   ☐ Supplemental

Will this project be submitted to additional funding sources? Yes __X__   No ____

(If the answer is Yes, identify funding sources, acct. no./grant no., and title of that project (if known).

Funding Source __NIH (Submission by 10/1/88)__ Acct. No. _____ Grant No. _____

Title _____

Funding Source _____ Acct. No. _____ Grant No. _____

Title _____

Funding Source _____ Acct. No. _____ Grant No. _____

Title _____

IV. Species/Strain of Animals

	Number/Type — 1st Yr. Total			number/type-Proj. Period		
	A	B	C	A	B	C
Adult dogs		65			190	

V. Is survival surgery required in this project? Yes __X__   No ____

If yes, where will surgery be performed? __Surgery Suite at Nora Eccles Harrison Cardiovascular Research & Training Institute__

VI. Where will animals be housed? __Animal Resources Center__   How long __7 to 10 days__

Is this an IACUC approved animal facility? Yes __X__   No ____

VII. Please attach a detailed narrative description of your proposed research.

VIII.   **PRINCIPAL INVESTIGATOR ASSURANCE**

I agree to abide by the provisions of the NIH Guide for the Care and Use of Laboratory Animals, the Public Health Service Policy on Humane Care and Use of Laboratory Animals and by the University of Utah Code of Ethics for the Use of Animals in Research. *I will make every effort to minimize the number of animals used by 1) avoiding unnecessary replication of previous experiments, 2) by using non-animal models when possible, and 3) by consulting biomedical research and other information sources.* I will permit emergency veterinary care to animals showing evidence of pain or illness. The information provided above is accurate to the best of my knowledge. If the data above relating to TYPE B or C procedures should require revision, I will so inform the Director of Animal Resources or other appropriate members of the Animal Care Committee.

Bruno Taccardi   6 September 1988   _Patricia Berger_   9-27-88

Signature of Principal Investigator   Date   IACUC Chairman or Designee   Date

Forward all copies for approval to Chairman, IACUC

P. J. BERGER
CHAIRMAN, IACUC
131-B SOUTH BIOLOGY

I.R.B.# __485__

REVIEW COMMITTEE FOR RESEARCH WITH HUMAN SUBJECTS
INSTITUTIONAL REVIEW BOARD - UNIVERSITY OF UTAH
Annual Request for Reapproval of a Continuing Project*

1. TITLE (also attach a copy of your last approval and consent document):

   Body Surface Cardiac Potential Mapping

2. AMENDMENTS SINCE LAST APPROVAL:

   None

   Have these changes been approved by the I.R.B.? ___Yes _____Date of approval
   ___No

3. NUMBER OF SUBJECTS ENTERED TO DATE: __136__

4. NUMBER OF SUBJECTS CURRENTLY ACTIVE IN STUDY: ___65___

5. DESCRIPTION OF EXPERIENCES (Benefits, Adverse Reactions, Withdrawals, Etc.):

   No subjects have declined participation or withdrawn before recording was complete. No adverse reactions are known to have occurred. Body surface maps are now used as part of evaluation in selected arrhythmia patients.
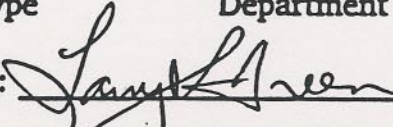
6. RESULTS TO DATE (if available):

   Body surface map features are helpful in dx and Rx of WPW patients and other selected arrhythmia patients.

7. TO DATE, DO BENEFITS OUTWEIGH RISKS? _X_Yes ___No ___Unknown

8. SPONSORING AND/OR CONTRACTING AGENCY: Treadwell Foundation Contract # __None__

9. PRINCIPAL INVESTIGATOR: __Larry S. Green__   __Cardiology__   __1-8183__
   Print or Type   Department   Telephone

10. PRINCIPAL INVESTIGATOR'S SIGNATURE: _Larry Green_   __10-4-90__
    Date

Your project has been REAPPROVED by the Health Sciences I.R.B., who have determined that this project is:

___High Risk _X_Moderate Risk ___Minimal Risk
___No Risk ___Exemption 46.101(b) Paragraph ___

__10-17-90__   _Keith G. Tolman_
Date Approved   Keith G. Tolman, M.D., Chairman

Continuing Review Scheduled for: October 17, 1991

* This form satisfies the annual questionnaire required by the General Assurance.
(0982H-4)   (Rev. 10/89)

I.R.B.# 2232

REVIEW COMMITTEE FOR RESEARCH WITH HUMAN SUBJECTS
INSTITUTIONAL REVIEW BOARD - UNIVERSITY OF UTAH
Annual Request for Reapproval of a Continuing Project*

1. TITLE (also attach a copy of your last approval and consent document):
   Estimation of Epicardial Potentials from Body Surface Maps

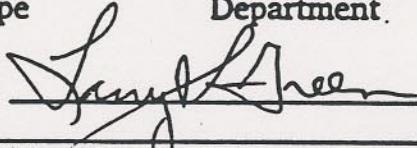2. AMENDMENTS SINCE LAST APPROVAL:
   None

   Have these changes been approved by the I.R.B.? ___Yes _____Date of approval
   ___No

3. NUMBER OF SUBJECTS ENTERED TO DATE: __12___

4. NUMBER OF SUBJECTS CURRENTLY ACTIVE IN STUDY: _4 (new)_

5. DESCRIPTION OF EXPERIENCES (Benefits, Adverse Reactions, Withdrawals, Etc.):
   No adverse experiences have occurred. One patient had mild claustrophobia during MRI.

6. RESULTS TO DATE (if available):
   3-Display images are available and additional patients will be collected to verify predicted potentials.
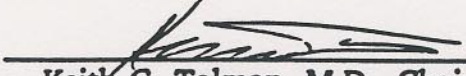
7. TO DATE, DO BENEFITS OUTWEIGH RISKS? _X_Yes ___No ___Unknown

8. SPONSORING AND/OR CONTRACTING AGENCY: Treadwell Foundation Contract # _None_

9. PRINCIPAL INVESTIGATOR: _Larry S. Green_   _Cardiology_   _1-8183_
                           Print or Type   Department   Telephone

10. PRINCIPAL INVESTIGATOR'S SIGNATURE: _Larry Green_   _10-4-90_
                                                           Date

Your project has been REAPPROVED by the Health Sciences I.R.B., who have determined that this project is:

___High Risk _X_Moderate Risk ___Minimal Risk
___No Risk ___Exemption 46.101(b) Paragraph ___

_10-17-90_
Date Approved   Keith G. Tolman, M.D., Chairman

Continuing Review Scheduled for: October 17, 1991

* This form satisfies the annual questionnaire required by the General Assurance.
(0982H-4)   (Rev. 10/89)

CC

PRINCIPAL INVESTIGATOR/PROGRAM DIRECTOR: __Johnson, Christopher R.__

Type the name of the Principal Investigator/Program Director at the top of each printed page and each continuation page.

TABLE OF CONTENTS

SECTION 3. Appendix *(Six collated sets. No page numbering necessary for Appendix)*

  Number of publications and manuscripts accepted for publication *(Not to exceed ten)*: __5__

  Other items *(list)*:

    Figures
    Mathematical Theory
    Letters from consultants

PHS 398 (Rev. 10/88)   Page 3*
*Number pages consecutively at the bottom throughout the application. Do *not* use suffixes such as 5a, 5b.

CC

A base salary is established in the first year for all personnel to be paid from the grant. Since the grant year would span two institutional fiscal years with merit salary increases anticipated at the beginning of each July, that base is calculated in the following manner: 4% over current rates for the first 7 months (December-June) and 4% over that figure for the remaining 5 months (July-November). That base salary is then increased 4% in each succeeding year.

In accordance with University of Utah guidelines, fringe benefits are set at 32.5% of salaries in all years.

Equipment

Item: *Macintosh IIci*

The procedure for converting the MRI images from the original digital form (from the Signa 7 MRI scanner) to pixel images that can be sampled and stored as surface coordinates requires a Macintosh II computer. The Macintosh II that we borrowed in the past to produce the digital-pixel conversions resides in another researcher's office and is primarily used for hardware data acquisition research (i.e. it is unavailable a large portion of the time).

Item: *Personal IRIS Workstation (Silicon Graphics 4D/35)*

Since the inverse problem is inherently three-dimensional, it is a necessity to view the data in its three dimensional form. The three dimensional output images consist of the model surfaces and volumes, potential distribution maps, and volume current density maps. The Evans and Sutherland Graphics computer that was used thus far cannot handle the large scale high resolution models, nor can it rotate rendered images. Software for this computer is only available for VAX/VMS host computers, is highly unportable and will soon be phased out in exchange for more standard and lower cost UNIX based equipment. A personal IRIS will provide a relatively low cost graphics workstation that can interface perfectly with the development tolls already existing on the larger 4D/VGX computer. The Silicon Graphics 4D/VGX, was obtained for another project and has only a single graphics terminal that is unavailable much of the time.

Item: *Apple Laserwriter IINT*

This will be used to obtain black and white hardcopy output from the Macintosh II and the Personal Iris Workstation.

Item: *Tektronix Color Phasor Printer*

This will be used to obtain color graphics hardcopy output from the Personal IRIS Workstation. Because of the complexity of the data, we will make extensive use of color to visualize our findings; this device will provide a permanent record of the results.

Supplies

Funds requested for supplies would be used for computer software, paper and tape. The amount requested is $1800 per year.

Travel

Funds of $1000 per year are requested to permit the principal investigator to attend one national scientific meeting per year. This would permit him to present project findings at an appropriate form and to participate in the discussion of other research in the field.

Other Expenses

Items in this category include the cost of repair and maintenance of project equipment, publication costs as well as reference books and journals. The amount requested is $762 in all years.

BIOGRAPHICAL SKETCH

Give the following information for the key personnel and consultants listed on page 2. Begin with the Principal Investigator/Program Director. Photocopy this page for each person.

NAME	POSITION TITLE	BIRTHDATE (Mo., Day. Yr.)
Johnson, Christopher R.	Research Assistant Prof. of Internal Medicine	January 17, 1960

EDUCATION (Begin with baccalaureate or other initial professional education, such as nursing, and include postdoctoral training.)

INSTITUTION AND LOCATION	DEGREE	YEAR CONFERRED	FIELD OF STUDY
Wright State University, Dayton, OH	B.S.	1982	Physics
University of Utah, Salt Lake City, UT	M.S.	1984	Physics
University of Utah, Salt Lake City, UT	Ph.D.	1990	Medical Biophysics

RESEARCH AND PROFESSIONAL EXPERIENCE: Concluding with present position, list, in chronological order, previous employment, experience, and honors. Include present membership on any Federal Government public advisory committee. List, in chronological order, the titles and complete references to all publications during the past three years and to representative earlier publications pertinent to this application. DO NOT EXCEED TWO PAGES.

RESEARCH AND/OR PROFESSIONAL EXPERIENCE:

Graduate Teaching Fellow, Department of Physics, University of Utah, Salt Lake City, Utah, 1982-1984

Engineering Physicist, Advanced Technology Division, Research and Development, Sperry Corporation (Unisys), Salt Lake City, Utah, 1984-1985

Assistant Professor of Physics, Westminster College, Salt Lake City, Utah, 1985-1989

Research Associate of Medicine, Nora Eccles Harrison Cardiovascular Research and Training Institute, University of Utah, Salt Lake City, Utah, 1989-1990

Research Assistant Professor of Medicine, Nora Eccles Harrison Cardiovascular Research and Training Institute, University of Utah, Salt Lake City, Utah, 1990-present

Adjunct Assistant Professor of Bioengineering, University of Utah, Salt Lake City, Utah, 1991-present

HONORS:

Siemens-Elma AB Young Investigator's Award, XVII International Congress on Electrocardiology, Florence Italy, 1990

2nd Prize winner of the IBM International Supercomputing Competition: Life and Health Sciences Division, 1989

Recipient of a Naomi Wehyer Faculty Award, Westminster College, 1987 (2 given per year)

Member of Sigma Pi Sigma (National Physics Honor Society)

Outstanding Teaching Award, Department of Physics, University of Utah, 1984

RMMC Mathematical Physics Scholarship

Former member of the Honors Faculty at Westminster College

BIBLIOGRAPHY:

1) Johnson CR: The generalized inverse problem in electrocardiography: theoretical, computational and experimental results. PHD Dissertation, March, 1990.

2) Johnson CR and Pollard AE: Electrical activation of the heart: computational studies of the forward and inverse problems of electrocardiography, Large Scale Analysis and Modeling MIT Press, Boston, pp 583-628, 1990.

3) Johnson CR: The generalized inverse problem in electrocardiography, Proc. of the 12th International IEEE/EMBS Conference on Biomedical Engineering, pp 593-594, 1990.

4) Johnson CR: Measurements of chaos in heart rhythms: Calculation of the Lyapunov exponent and fractal dimension, IEEE Trans. Biomed Eng, In press, 1990.

5) Johnson CR: The generalized inverse problem. J Electrocardiol. To be published July, 1991.

ABSTRACTS

1) Johnson CR: The generalized inverse problem. Proc. of the XVII International Congress on Electrocardiology and 31st International Symposium on Vectorcardiography, Florence, Italy, pp 245, 1990.

2) Pollard AE and Johnson CR: Large scale computer modeling of the electrical activity of the heart. Proc. of the SHARE Conference on Computing, pp 367, 1990.

3) Johnson CR, Ershler PR and MacLeod RS: Electrical current flow in the human thorax. IBM Supercomputing Competition, 1990 (submitted).

PHS 398 (Rev. 10/88)   Page 7 .   FF

*Number pages consecutively at the bottom throughout the application. Do not use suffixes such as 5a, 5b.

BIOGRAPHICAL SKETCH

Give the following information for the key personnel and consultants listed on page 2. Begin with the Principal Investigator/Program Director. Photocopy this page for each person.

NAME MacLeod, Robert S.	POSITION TITLE Research Associate	BIRTHDATE (Mo., Day, Yr.) August 22, 1955

EDUCATION (Begin with baccalaureate or other initial professional education, such as nursing, and include postdoctoral training.)

INSTITUTION AND LOCATION	DEGREE	YEAR CONFERRED	FIELD OF STUDY
Dalhousie University, Halifax, N.S., Canada	B.Sc.	1979	Engineering Physics
Technische Universität Graz, Austria	M.Sc.	1985	Electrical Engineering
Dalhousie University, Halifax, N.S., Canada	Ph.D.	1990	Physiology/Biophysic

RESEARCH AND PROFESSIONAL EXPERIENCE: Concluding with present position, list, in chronological order, previous employment, experience, and honors. Include present membership on any Federal Government public advisory committee. List, in chronological order, the titles and complete references to all publications during the past three years and to representative earlier publications pertinent to this application. DO NOT EXCEED TWO PAGES.

RESEARCH AND/OR PROFESSIONAL EXPERIENCE:

Summer Research Student, Department of Physiology and Biophysics, Dalhousie University, Halifax, N.S., Canada, 1977-79

Research Assistant and Computer System Manager, Institut für Medizinische, Physik und Biophysik, Graz, Austria

Postdoctoral Fellow, Nora Eccles Harrison Cardiovascular Research and Training Institute, University of Utah, Salt Lake City, Utah

HONORS

Dartmouth High School/Student Council Scholarship, 1974-75
Dalhousie University Academic Scholarships, 1975-79
Dalhousie University Medal in Engineering Physics, 1979
Austrian Student Union Scholarships, 1980-85
Izaak Walton Killam Memorial Scholarship, 1986-90
IODE War Memorial Postgraduate Scholarship, 1986-87
Medical Research Council of Canada Studentship, 1987-90
Heart and Stroke Foundation of Canada Postdoctoral Fellowships 1990-92

PUBLICATIONS

Diplomarbeit (Master's Thesis) Signal Verzögerung in der Tontechnik -- Entwicklung eines digitalen Verzögerungsgerätes mit Deltamodulatoren (1985).

Ph.D. Thesis Percutaneous Transluminal Coronary Angioplasty as a Model of Cardiac Ischemia: Clinical and Modelling Studies (1990)

Papers

1) Helppi, R.K., MacLeod, R. and Horacek, B.M.: Modular software for the processing of cardiac signals. *Proceedings of Computers in Cardiology,* pages 367-368, 1979.

2) MacLeod, R.S., Gardner, M.J., and Horacek, B.M., Hochauflösende EKG-Mapping-Verfahren für Untersuchungen während Koronardilitation. *Biomedizinische Technik* 15. Jahrestagung der Österreichischen Gesellschaft für Biomedizinische Technik, Innsbruck, Austria, 1990

3) MacLeod, R.S., Gardner, M.J., MacDonald, R.G., Henderson, M.A., Miller, R.M., and Horacek, B.M. Application of an inverse solution to body surface potential mapping during PTCA. In *IEEE Engineering in Medicine and Biology Society 12th Annual International Conference* , pages 633-534. IEEE Press, 1990.

4) MacLeod, R.S., Hoyt, B.K., Sherwood, J.D., MacInnis, P.J., Potter, R.V. and Horacek, B.M.: A body surface mapping unit for recording during coronary angioplasty. In *IEEE Engineering in Medicine and Biology Society 10th Annual International Conference*, pages 97-98. IEEE Press, 1988

5) Montague, T.J., Witkowski, F.X., Miller, R.M., Henderson, M.A., MacDonald, R.G., MacLeod, R.S., Gardner, M.J. and Horacek, B.M. Persistent changes in the body surface electrocardiogram following successful coronary angioplasty. *J Electrocardiol.* (In Press).

Abstracts, Posters

1) MacLeod, R.S., Gardner, M.J., and Horacek, B.M., Body surface mapping of angioplasty-induced ischemia. *J. Mol. & Cell. Cardiol..* International Society for Heart Research, XI European Meeting, Glasgow, United Kingdom, 1990

Number pages consecutively at the bottom throughout the application. Do not use suffixes such as 5a, 5b.

BIOGRAPHICAL SKETCH

Give the following information for the key personnel and consultants listed on page 2. Begin with the Principal Investigator/Program Director. Photocopy this page for each person.

NAME Ershler, Philip R.	POSITION TITLE Research Assistant Professor	BIRTHDATE *(Mo., Day, Yr.)* November 18, 1950

EDUCATION *(Begin with baccalaureate or other initial professional education, such as nursing, and include postdoctoral training.)*

INSTITUTION AND LOCATION	DEGREE	YEAR CONFERRED	FIELD OF STUDY
Colorado College, Colorado Springs, CO	BS	1972	Mathematics
University of Utah, Salt Lake City, UT	MS	1975	Electrical Engineering
University of Utah, Salt Lake City, UT	PhD	1986	Electrical Engineering

RESEARCH AND PROFESSIONAL EXPERIENCE: Concluding with present position, list, in chronological order, previous employment, experience and honors. Include present membership on any Federal Government public advisory committee. List, in chronological order, the titles and complete references to all publications during the past three years and to representative earlier publications pertinent to this application. DO NO EXCEED TWO PAGES.

RESEARCH AND/OR PROFESSIONAL EXPERIENCE:

Artificial Organs, University of Utah Medical Center, Salt Lake City, Utah, June 1969 - August 1969
Biomedical Instrumentation, Holy Cross Hospital, Salt Lake City, Utah, June 1971 - August 1971
Biophysics and Bioengineering, University of Utah, Salt Lake City, Utah, June 1970 - August 1970
Data Reduction, Litton Industries, Salt Lake City, Utah, June 1972 - September 1972
Electrical Engineer, Nora Eccles Harrison Cardiovascular Research and Training Institute, University of Utah, Salt Lake City, Utah, September 1973 to November 1986
Research Assistant Professor, Department of Internal Medicine and Nora Eccles Harrison Cardiovascular Research and Training Institute, University of Utah School of Medicine, Salt Lake City, Utah, November 1986 to present

PUBLICATIONS:

1) Ershler PR, Lux RL, Green LS, Caputo GR and Parker D: Determination of 3-dimensional torso, heart and electrode geometries from magnetic resonance images. In Proceedings 10th Annual Conference IEEE Engineering in Medicine and Biology 10: 0121-0122, 1988

2) Lux RL, Ershler PR and Taccardi B: 3-dimensional displays of isochrone and isopotential surfaces. In Proceedings 10th Annual Conference IEEE Engineering in Medicine and Biology 10:0108-0109, 1988

3) Macchi E, Ershler P, Lux R and Taccardi B: On-line mapping of three-dimensional time varying bioelectric fields. In Proceedings 10th Annual Conference IEEE Engineering in Medicine and Biology 10:0115-0116, 1988

4) Lux RL, Ershler PR, Anderson KP and Mason JW: Rapid localization of accessory pathways in WPW syndrome using unipolar potential mapping. 11th International Conference IEEE/EMBS, 11(1):195-196, 1989

5) Burgess MJ, Lux RL and Ershler PR: Estimation of depth of onset of activation from cardiac surface electrograms. Circulation 80:42, 1989

6) Taccardi B, Green LS, Ershler PR and Lux RL: Epicardial potential mapping: effects of conducting media. Circulation 80:134, 1989

7) Taccardi B, Lux RL, Ershler PR, Watabe S and Macchi E: Normal and abnormal intramural spread of excitation and associated potential distributions. XVII International Congress on Electrocardiology, p 12, 1990. Presented at the 31st International Symposium on Vectorcardiography, Florence, Italy, 9/26-29/90.

BIOGRAPHICAL SKETCH

Give the following information for the key personnel and consultants listed on page 2. Begin with the Principal Investigator/Program Director. Photocopy this page for each person.

NAME	POSITION TITLE	BIRTHDATE (Mo., Day, Yr.)
Taccardi, Bruno	Research Professor of Internal Medicine	October 12, 1922

EDUCATION (Begin with baccalaureate or other initial professional education, such as nursing, and include postdoctoral training.)

INSTITUTION AND LOCATION	DEGREE	YEAR CONFERRED	FIELD OF STUDY
State University of Milan, Milano, Italy	M.D.	1946	Medicine
Agrege, University of Brussels Belgium	Ph.D.	1951	Physiology
Libero Docente, University of Pavia, Italy	Ph.D.	1961	Physiology

RESEARCH AND PROFESSIONAL EXPERIENCE: Concluding with present position, list, in chronological order, previous employment, experience, and honors. Include present membership on any Federal Government public advisory committee. List, in chronological order, the titles and complete references to all publications during the past three years and to representative earlier publications pertinent to this application. DO NOT EXCEED TWO PAGES.

RESEARCH AND/OR PROFESSIONAL EXPERIENCE:

Assistant Professor, (Part time) University of Pavia, 1964-1975

Assistant, University of Brussels, 1948-1951

Chef de Travaux, University of Brussels, 1951-1959

Director, Electrophysiological Laboratory, Simes Institute for Experimental Cardiology, Milan, 1959-1975

Director, Institute of General Physiology, University of Parma, 1976-1987

Professor, General Physiology, University of Catania, 1975-1976

Professor, General Physiology, University of Parma, 1976 to January 1989

Visiting Professor of Internal Medicine, University of Utah School of Medicine, July-September 1985 and November 1986-February 1989

Research Professor of Internal Medicine, University of Utah School of Medicine, February 1989 to present

HONORS:

Winner, International Honeywell Prize, 1980

Doctor Honoris Causa, University of Caen (France), 1981

Gold medal of the President of the Italian Republic for scientific merit, 1982

Winner, Professor Pierre Rijlant Triennial Prize for Cardiac Electrophysiology Brussels, 1989

PUBLICATIONS:

1) Macchi E, Arisi G and Taccardi B: Intracavitary mapping: An improved method for locating the site of origin of ectopic ventricular beats by means of a mathematical model. Proc IEEE Engineering in Medicine and Biology Society 10th Ann Intl Conf, New Orleans, November 4-7, 1988, pp 187-188

2) Macchi E, Ershler PR, Lux RL and Taccardi B: On-line mapping of three-dimensional time varying bioelectric fields. Proc IEEE Engineering in Medicine and Biology Society 10th Ann Intl Conf, New Orleans, November 4-7, 1988, pp 115-116

3) Lux RL, Ershler PR and Taccardi B: 3-dimensional displays of isochrone and isopotential surfaces. Proc IEEE Enginering in Medicine and Biology Society 10th Ann Intl Conf, New Orleans, November 4-7, 1988, pp 108-109

4) De Ambroggi L, Musso E and Taccardi B: Body surface mapping. Chapter 27 In: Comprehensive Electrocardiology, Theory & Practice in Health & Disease, PW Macfarlane & TDV Lawrie, eds. Pergamon Press, New York, 1989, pp 1015-1049

5) Arisi G, Macchi E, Passolunghi P and Taccardi B: Resolving power of an intraventricular probe for detecting the site of origin of ectopic ventricular beats. In "Electrocardiology 1988", H. Abel, editor, Excerpta Medica, Amsterdam, 1989, pp 217-220

6) Taccardi B, Lux RL, Ershler PR, Steadman B and Watabe S: Intracardiac and extracardiac potential distributions during ventricular ectopic beats. Proc IEEE Engineering in Medicine and Biology Society 11th Annual Int'l Conf, Seattle, WA, Vol 11:197-198, 1989

7) Macchi E, Arisi G, Colli-Franzone P, Guerri L, Olivetti G and Taccardi B: Localization of ventricular ectopic beats from intracavitary potential distributions: An inverse model in terms of sources. Proc IEEE Engineering in Medicine and Biology Society 11th Annual Int'l Conf, Seattle, WA, Vol 11:191-192, 1989

*Number pages consecutively at the bottom throughout the application. Do not use suffixes such as 5a, 5b.

BIOGRAPHICAL SKETCH - Bruno Taccardi, MD, PhD

8) Taccardi B, Lux R, Ershler P, Watabe S, Macchi E: Intramural spread of excitation wavefronts and associated potential fields. In "Advances in Electrocardiology", Z. Antaloczy et al, Editors, Elsevier, Amsterdam, 1990, pp 61-62

9) Watabe S, Taccardi B, Lux RL and Ershler PR: Effect of non-transmural necrosis on epicardial potential fields: correlation with fiber direction. Circulation 82:S2115-2127, 1990

10) Taccardi B: Body surface mapping and cardiac electric sources: A historical survery. J Electrocardiol, 1990 (In press)

11) Taccardi B: Three-dimensional spread of excitation in the ventricles. Invited paper. Giornate Internazionali Di Chirvrgia, E. Malan, Parma, September, 1990 (In press).

ABSTRACTS:

1) Taccardi B, Watabe S, Ershler P, Lux R and Macchi E: A method for separating the axial and transverse contribution of excitation wavefronts to the cardiac electric field. Circulation 78 (Suppl II): 412, 1988 .

2) Kornreich F, Montague T, Rautaharju P, Kavadias M and Taccardi B: Diagnostic body surface potential map patterns in left ventricular hypertrophy. Circulation 78 (Suppl II): 34, 1988.

3) Taccardi B, Lux RL, Ershler PR and Watabe S: Intramural spread of excitation wavefronts and associated potential fields. 16th International Congress on Electrocardiology, Budapest, Hungary, September 3-7, 1989

4) Watabe S, Taccardi B, Lux RL Ershler PR: Effect of non-transmural necrosis on epicardial potential fields: correlation to intramural fiber direction. Circulation 80-II:135, 1989

5) Taccardi B, Green LS, Ershler PR and Lux RL: Epicardial potential mapping: Effects of conducting media. Circulation 80-II:134, 1989

6) Taccardi B, Lux RL, Ershler PR, Watabe S and Macchi E: Normal and abnormal intramural spread of excitation and associated potential distributions. XVII International Congress on Electrocardiology, p 12, 1990. 31st International Symposium on Vectorcardiography, Florence, Italy, 9/26-29/90

7) Taccardi B, Watabe S, Lux RL, Ershler PR and Macchi E: Effect of myocardial anisotropy and nonhomogeneous conducting media on intracardiac and epicardial potential fields. XVII International Congress on Electrocardiology, p 8, 1990. 31st International Symposium on Vectorcardiography, Florence, Italy, 9/26-29/90

8) Cola GD, Guerri L, Macchi E, Pennacchio M and Taccardi B: Numerical simulation of electric fields generated by dipolar sources in tridimensional anisotropic non homogeneous media. XVII International Congress on Electrocardiology, p 226, 1990. 31st International Symposium on Vectorcardiography, Florence, Italy, 9/26-29/90.

BIOGRAPHICAL SKETCH

Give the following information for the key personnel and consultants listed on page 2. Begin with the Principal Investigator/Program Director. Photocopy this page for each person.

NAME	POSITION TITLE	BIRTHDATE (Mo., Day, Yr.)
Green, Larry S.	Associate Professor of Medicine	August 2, 194?

EDUCATION *(Begin with baccalaureate or other initial professional education, such as nursing, and include postdoctoral training.)*

INSTITUTION AND LOCATION	DEGREE	YEAR CONFERRED	FIELD OF STUDY
University of Utah, Salt Lake City, Utah	BS	1969	Biology
University of Utah College of Medicine, Salt Lake City, Utah	MD	1973	Medicine

RESEARCH AND PROFESSIONAL EXPERIENCE: Concluding with present position, list, in chronological order, previous employment, experience, and honors. Include present membership on any Federal Government public advisory committee. List, in chronological order, the titles and complete references to all publications during the past three years and to representative earlier publications pertinent to this application. DO NOT EXCEED TWO PAGES.

RESEARCH AND PROFESSIONAL EXPERIENCE

Research Trainee in Cardiac Electrophysiology, 1972-1973, Wilhelmina Gausthaus, University of Amsterdam, Netherlands, Dirk Durrer, M.D., Preceptor, and University of Utah College of Medicine, Salt Lake City, Utah, J.A. Abildskov, M.D., Preceptor

Intern in Medicine, 1973-1974, Duke University Medical Center, Durham, North Carolina

Resident in Medicine, 1974-1975, Duke University Medical Center, Durham, North Carolina

Fellow in Cardiology, 1975-1976, Duke University Medical Center, Durham, North Carolina

Chief Resident in Medicine, 1976-1977, University of Utah Medical Center, Salt Lake City, Utah

Postdoctoral Fellow in Cardiology, 1977-1978, University of Utah Medical Center, Salt Lake City, Utah

Director, Heart Station, 1978-80, Louisiana State University Medical Center, Shreveport, Louisiana

Assistant Professor of Medicine, 1978-1980, Louisiana State University School of Medicine, Shreveport, Louisiana

Assistant Professor of Internal Medicine, 1980-1986, University of Utah College of Medicine, Salt Lake City, Utah

Cardiology Consultant, 1982, Hill Air Force Base Hospital, Layton, Utah

Associate Professor of Internal Medicine, 1986-present, University of Utah College of Medicine, Salt Lake City, Utah

HONORS

Phi Kappa Phi

Outstanding Medical Student Research Award, 1973, University of Utah

Outstanding Teacher Award, 1979, Louisiana State University School of Medicine

SELECTED PUBLICATIONS

1) Abildskov JA and Green LS: The recognition of arrhythmia vulnerability by body surface electrocardiographic mapping. AM Heart Assoc "State of the Art Consensus Conference on Electrophysiological Testing in the Diagnosis and Treatment of Patients with Cardiac Arrhythmias," Sept 85). Circulation 75(Suppl III): 79-83, 1987

2) Green LS, Lux RL, Stilli D, Haws CW and Taccardi B: Fine detail in body surface potential maps: Accuracy of maps using a limited lead array and spatial and temporal data representation. J Electrocardiol 20(1):21-26, 1987

3) Haws CW, Green LS, Burgess MJ and Abildskov JA: Effects of cardiac sympathetic nerve stimulation on regional coronary blood flow. Am J Physiol 252 (Heart & Circ Physiol 21):H269-H274, 1987

*Number pages consecutively at the bottom throughout the application. Do not use suffixes such as 5a, 5b.

4) Freedman RA, Anderson KP, Green LS and Mason JW: Effect of erythromycin on ventricular arrhythmias and ventricular repolarization in idiopathic long QT interval syndrome. Am J Cardiol 59-1:168-169, 1987

5) Kozmann G, Lux RL and Green LS: Application of non-parametric methods for identifying discriminative information in body surface maps. In Proceedings IEEE/Ninth Annual Conference of the Engineering in Medicine and Biology Society, 1987, pp 1873-1874

6) Green LS, Lux RL and Haws CW: Detection and localization of coronary artery disease with body surface mapping in patients with normal electrocardiograms. Circulation 76:1290-1297, 1987

7) Abildskov JA, Burgess MJ, Millar CK, Fruehan CT, Wyatt RF and Green LS: The distributed character of ventricular recovery as a factor in electrocardiography and vectorcardiography. In Vectorcardiography-2, I Hoffman and E Glassman, eds. Amsterdam, North-Holland Publ Co, 1971, pp 651-655

8) Burgess MJ and Green LS: Ventricular recovery properties and their relation to the body surface electrocardiogram. Chapter 3 In Pediatric and Fundamental Electrocardiology, J Liebman, R Plonsey, and Y Rudy, eds. Boston, Martinus Nijhoff publishing, 1987, pp 39-48

9) Abildskov JA, Green LS and Lux RL: Detection of disparate ventricular repolarization by means of the body surface electrocardiogram. In Cardiac Electrophysiology and Arrhythmias, DP Zipes and J Jalife, eds New York, Grune and Stratton, Inc, 1985, pp 495-499

10) Green LS, Lux RL, Haws CW, Burgess MJ and Abildskov JA: Features of body surface maps from a large normal population. In Electrocardiographic Body Surface Mapping, R Th van Dam, A van Oosterom, eds Dordrecht Martinus Nijhoff, 1986

11) Lux RL, Green LS, Haws CW, Burgess MJ and Abildskov JA: Use of orthonormal expansions for representing body surface potential maps. In Electrocardiographic Body Surface Mapping, R Th van Dam, A van Oosterom, eds Dordrecht Martinus Nijhoff, 1986

12) Lux RL, Green LS and Haws CW: Validating a coronary artery disease detection scheme. In Computerized Interpretation of the Electrocardiogram, Proc of the 1986 Engineering Foundation Conference, April 7-10, 1986, Santa Barbara CA. New York, Engineering Foundation, 1987, pp 138-141

13) Green LS, Lux RL and Haws CW: Detection and localization of coronary artery disease with body surface mapping in patients with normal electrocardiograms. Circulation 76:1290-1297, 1987

14) Kozmann G, Lux RL and Green LS: Some properties of the probability distributions of body surface maps from clinically normal groups. In Proc 15th International Congr Electrocardiol, Wiesbaden, Aug 17-19, 1988. Elsevier, Amsterdam, 1989, pp 227-230

15) Kozmann G, Lux RL and Green LS: Sources of variability in normal body surface maps. Circulation 79:1077-1083, 1989

16) Mirvis DM, Berson AS, Goldberger AL, Green LS, Neger JJ, Hinohara T, Insel J, Krucoff MW, Moncrief A, Selvester RH and Wagner GS: Instrumentation and practice standards for electrocardiographic monitoring in special care units. Circulation 79:464-471, 1989

17) Abildskov JA and Green LS: Long QT Syndromes. In Advances in Cardiac Electrophysiology and Arrhythmias. C Fisch and B Surawicz, eds. In press, 1990

OTHER SUPPORT

(Use continuation pages if necessary)

FOLLOW INSTRUCTIONS CAREFULLY. Incomplete, inaccurate, or ambiguous information about OTHER SUPPORT could lead to delays in the review of the application. OTHER SUPPORT to be listed here refers to all current or requested support whether related to this application or not. If there are changes subsequent to submission, notify the executive secretary of the initial review group.

For each of the key personnel named on page 2, list, in three separate groups: (1) *all* currently active support; (2) *all* applications and proposals pending review or funding; and (3) applications and proposals planned or being prepared for submission. Include *all* Federal, non-Federal (e.g., for-profit, pharmaceutical, foundations), and institutional research, training, and other grant, contract, and fellowship support at the applicant organization and elsewhere. If part of a larger project, identify the principal investigator/program director and provide the data for both the parent project and the subproject. If none, state "none."

For *each* item give: (a) the source of support, identifying number and title; (b) percentage of appointment on the project; (c) dates of entire project period; (d) annual direct costs; (e) a brief description of the project; (f) whether the item overlaps, duplicates, or is being replaced or supplemented by the present application; delineate and justify the nature and extent of any scientific and/or budgetary overlaps or boundaries; and (g) any modifications that will be made should the present application be funded.

PRINCIPAL INVESTIGATOR/PROGRAM DIRECTOR: **Christopher R. Johnson**
(1) CURRENTLY ACTIVE SUPPORT: (a)

- a) National Heart, Lung & Blood Institute, NIH
  ID number: RO1 HL42388-03
  Title: Cardiac Electrophysiologic Imaging from Potential Fields
  PI: Robert L. Lux
- b) % appointment: 40% as Collaborating Investigator
- c) Entire project period: 4/1/89-3/31/94
- d) Annual direct costs: $148,994
- e) Description: Project objective is to develop and evaluate improved methods for providing robust estimates of spatial distributions of cardiac electrophysiologic properties from extracellular potential fields.
- f) Scientific or budgetary overlap, replacement, duplication or supplement: None
- g) Modifications required if present application funded: None

2) **Pending review or funding:**
- a) Source: John Simon Guggenheim Memorial Foundation
  ID number: None
  Title: Supercomputing in Electrocardiology
  Fellowship Candidate: Christopher R. Johnson
- b) % appointment: Not applicable - see description
- c) Entire project period: 3/1/91-2/28/92
- d) Annual direct costs: To be determined at time of award (preceding year recipients averaged $26,329)
- e) Description: The fellowships were established to assist research and artistic creation. The fellowships are open to all fields of knowledge and creation in the arts. The one-time award is made directly to the individual (who must pay taxes on it) and can be used at the discretion of the awardee and the foundation for travel expenses, publication costs, partial salary support, etc.
- f) Scientific or budgetary overlap, replacement, duplication or supplement: None
- g) Modifications required if present application funded: None

3) **Planned or Being Prepared for Submission:** None

Robert S. MacLeod
1) **Currently active support:**
- a) Source: Heart and Stroke Foundation of Canada
  ID number: None
  Title: Research Fellowship
- b) % appointment: No set amount - see description
- c) Entire period of support: 7/1/90-6/30/92
- d) Annual direct costs: Canadian $24,389

Robert S. MacLeod *continued*
- e) Brief description: This is a postdoctoral fellowship requiring at least a 75% commitment of effort to the study of three-dimensional modeling and display of cardiac potential fields as well as body surface mapping using balloon angioplasty. It is renewable for a second year.
- f) Scientific or budgetary overlap, replacement, duplication or supplement: This fellowship will end in June 1992, the first year of the present application. During this time, Dr. MacLeod's effort will be 20% to eliminate any budgetary overlap.
- g) Modifications if present application funded: None
2) **Pending review or funding:** None
3) **Planned or being prepared for submission:** None

Philip R. Ershler
1) **Currently active support:**
- a) Source: National Institutes of Health
  ID number: 5 RO1 HL34288-05
  Title: Effects of Activation Order on Repolarization
  PI: M.J. Burgess
- b) % appointment: 30% as coinvestigator
- c) Entire period of support: 9/1/85-8/31/91
- d) Annual direct costs: $192,412
- e) Brief description: Studies to determine the factors responsible for electrotonic modulation of repolarization properties by activation sequence and the relation of such modulations to vulnerability to arrhythmias.
- f) Overlap etc: None
- g) Modifications if present application funded: None
2) **Pending Review or Funding**
- a) Source: National Institutes of Health
  ID number: 2 RO1 HL34288-06A1
  Title: Effects of Activation Order on Repolarization
  PI: M.J. Burgess
- b) % appointment: 30% as coinvestigator
- c) Entire period of support: 9/1/91-8/31/96
- d) Annual direct costs: $252,335
- e) Brief description: Renewal application of grant number 5 RO1 HL34288-05 cited above
- f) Overlap etc: None
- g) Modifications if present application funded: None
3) **Planned or being prepared for submission:** None

RESOURCES AND ENVIRONMENT

FACILITIES: Mark the facilities to be used at the applicant organization and briefly indicate their capacities, pertinent capabilities, relative proximity and extent of availability to the project. Use "other" to describe the facilities at any other performance sites listed in Item 9, page 1, and at sites for field studies. Using continuation pages if necessary, include an explanation of any consortium/contractual arrangements with other organizations.

☐ Laboratory: The CVRTI houses five animal laboratories (300 sq. ft./lab), each containing resources for acute whole animal experiments, including dog tables, respirators, 6 channel programmable stimulators, surgical instruments, direct lines connecting the laboratory to the computer facility such that data can be analyzed on line, and ten channel recording systems for monitoring and recording ECG's, blood pressure and flow, heart rate and temperature.

☐ Clinical: Not Applicable

☐ Animal: The University of Utah Vivarium is a fully accredited animal care facility directed by a full time veterinarian. Animals to be used in the proposed experiments will obtained, housed, prepared, and transported by Vivarium personnel.

☐ Computer: The CVRTI supports a DEC VAX 750 (6 Mbytes of memory, 1.3 Gbytes of disk space, 2 digital magnetic tape systems, 2 electrostatic printer plotters and 15 terminals), a DEC MicroVax II (2 Mbytes of memory, 160 Mbytes of disk space), 6 Macintosh personal computers, and a Silicon Graphics 4D/210 VGX Workstation (32 Mbytes of memory, 780 Mbytes disk space). The CVRTI also has a fiber optic connection to a campus wide network which provides access to the IBM 3090/600S supercomputer.

☐ Office: Sufficient office space (approx. 100 sq. ft./researcher) is available to the investigators of the CVRTI. Two full time secretaries and an administrative assistant to the director provide all the necessary support for grants administration, manuscript preparation, etc.

☐ Other (_____):

MAJOR EQUIPMENT: List the most important equipment items already available for this project, noting the location and pertinent capabilities of each.

An electrolytic tank that exhibits realistic geometry. The tank consists of 1302 measurement electrodes, of which 384 reside on the torso surface, 180 are positioned just outside the epicardial surface, and the remaining 738 fill the volume. Three 64 - channel and one 192 - channel multiplexer recording systems are available for mapping and tank studies. The recording systems feature switch selectable gain for maximizing signal to noise ratio during recording, flexible recording formats, and on-line, real time monitoring of signals.

ADDITIONAL INFORMATION: Provide any other information describing the environment for the project. Identify support services such as consultants, secretaries, machine shop, and electronics shop, and the extent to which they will be available to the project.

Proposed research will be carried out at the Cardiovascular Research and Training Institute (CVRTI) of the University of Utah. There are 17 senior investigators at the CVRTI representing research disciplines of cardiac electrophysiology at the organ, cellular, and molecular levels. Facilities include laboratory and office space, 1130 sq. ft. of electronic and machine shop space, and computational resources.

SECTION 2. RESEARCH PLAN

A. SPECIFIC AIMS

The overall goal of this research is the development and validation of improved methods for computing epicardial potential distributions, isochrones, and electrograms from body surface potentials. These methods will be used to characterize normal and abnormal electrical cardiac behavior noninvasively through an inverse procedure. The utility of the inverse procedure depends ultimately on the degree of accuracy and spatial resolution with which epicardial potentials can be recovered. We propose to apply theoretical studies, computational simulations, and animal experiments to establish the limits of accuracy and spatial resolution of the inverse procedure.

Specifically, by comparing potential distributions gathered from experiments using a reralistically shaped electrolytic tank with those obtained from simulations using a computer model which is the computational equivalent of the electrolytic tank, we will be able to quantitatively measure how the accuracy of electrocardiographic forward and inverse problems depend on the resolution of the geometric model, inclusion of anisotropic inhomogeneities, and the numerical techniques employed. Furthermore, we propose to use computer models based entirely on human data to evaluate the utility of the inverse procedure for specific pathologies.

A solution to the inverse problem in electrocardiography would provide a noninvasive means for the evaluation of myocardial ischemia, the localization of the site of origin of ventricular arrhythmias and the site of accessory pathways in Wolff-Parkinson-White (WPW) syndrome, and, more generally, the determination of patterns of excitation and of recovery of excitability.

The key questions to be answered are whether one can recover epicardial potentials at a high enough resolution to be clinically useful, and, if so, how much of the complexity of the torso and its tissue structure - inhomogeneity and anisotropy of the muscle, fat and lung volumes - must be determined or estimated in order to obtain such information. The answers to these questions depend primarily on several features of the problem: geometry of the thorax and its internal structures; conductivity of tissues, including direction; numerical solution techniques, particularly regularization of the resulting mathematically ill-posed problem; and measurement of the body surface potential distribution.

The importance of the geometric relationship between torso and epicardial surfaces is clear [1,2]; what is not clear is, quantitativley, what functional relationship exists between the spatial resolution of the reconstructed geometry and the accuracy of the recovered epicardial potentials. A hypothesis to be tested is that *it is possible to determine the spatial resolution required in the geometric model to achieve a given accuracy of the inverse solution.*

There have been several studies which demonstrate the importance of including inhomogeneity in the volume conductor model used for inverse solutions [3,4,5]; what has not been stressed is, quantitatively, what effects the anisotropy of the skeletal muscle and the inhomogeneous lung and fat volumes have on the accuracy of recovered epicardial potentials. Another hypothesis to be tested is that *incorporation of the anisotropic skeletal muscle and the inhomogeneous lung and fat volumes into a geometrically realistic computer model will increase the accuracy, and the spatial resolution of the inverse procedure.* The ability to assess the importance of tissue conductivity in the inverse procedure requires a solution method which can incorporate the structure and, if necessary, the anisotropic nature of internal inhomogeneities in a physiologically realistic manner. The only numerical technique which allows for this constraint - and the technique which will be used in this study - is the finite element method. A corallary hypothesis to be tested is that the *assignment of anisotropic conductivities such as that of skeletal muscle can be modeled effectively*

by discretizing the internal tissue structure using a fine mesh of tetrahedra and then assigning to each individual tetrahedron a directional conductivity tensor.

While the numerical difficulties of the inverse problem are many and varied, perhaps the two most important are, first, the solution of the large systems of equations, and second, the regularization of the resulting mathematically ill-posed problem. It is clear that the two largest sources of errors in the recovery of epicardial potentials are caused by measurement of the body surface potentials and discretization of the thorax geometry [6,7,8]. Therefore, the hypothesis to be tested here is that *the development of a more comprehensive approach to regularization based upon the concept of an error vector which weights individual sources of error will provide for a more accurate estimate of epicardial potentials.*

B. BACKGROUND AND SIGNIFICANCE

Electrocardiography has played an important role in the detection and characterization of heart disease. Inverse electrocardiography has as its goal the determination of cardiac electrical events from noninvasive electrical measurements taken on the body surface. A solution to the inverse problem, if accomplished with high enough resolution, would allow for a clinically useful noninvasive procedure to estimate the electrophysiological state of the heart. Current knowledge pertaining to inverse procedures yields a wealth of information on methods, strategies, and techniques. Yet much of this information has not addressed the applications and clinical utility of the inverse procedure in a realistic way. This brings into focus the major issues to be addressed in the proposed research, specifically, **while previous treatments of the inverse problem have addressed many important aspects of the procedure, there has not been a comprehensive quantitative treatment of the physical and mathematical difficulties associated with a large scale model that contains realistic geometry, anisotropy, and inhomogeneity in such a way that researchers can evaluate the ultimate clinical utility of such an approach.** The overall goal of this study is to establish, quantitatively, the limits of accuracy and spatial resolution* of the inverse procedure, using an electrolytic tank that exhibits realistic geometry and computer models that incorporate information derived entirely from human sources. Accomplishing the goal of this study requires the characterization, theoretical simulation, and experimental validation of the individual effects of anisotropic inhomogeneity, geometrical complexity, and numerical techniques on the recovery of epicardial potential distributions.

The inverse problem in electrocardiography is a mathematical description that relates electric potentials measured on the body surface to the electrical activity within the heart, while the goal of the forward problem is to determine the electrical behavior on and within the thorax from known cardiac sources. In general, the inverse problem is not uniquely solvable, because the primary cardiac sources that produce the electric fields are, at this time, inaccessible. Consequently, a single set of body-surface potentials can yield multiple inverse solutions. Historically, the problem of nonuniqueness has been circumvented using various equivalent source models. These models generally fall into one of two categories: idealized heart sources, such as dipole and multiple-dipole models [9,10]; and measurable heart sources, such as epicardial potentials [11,12]. All the different varieties of discrete heart-source models in the first group share a common problem: the impossibility of direct experimental validation. On the other hand, the formulation in terms of epicardial potentials avoids this problem: besides allowing for direct experimental validation - a

---

* For our purposes we define accuracy in the global sense - as the ability of the inverse solution to reproduce the actual epicardial potential distribution; in the local sense, we define spatial resolution as the ability of the inverse solution to resolve individual events which are in close spatial proximity. These measures are quantified in the Methods section.

necessity for measuring the accuracy of recovered epicardial potentials - the inverse problem in terms of epicardial potentials is unique [13], that is, there exists theoretically only one correct solution. Even though the transfer matrix relating the body-surface and epicardial potentials is unique, due to the internal inhomogeneities, anisotropies, and complex geometry of the volume conductor (thorax), any direct attempt to recover epicardial potentials from body-surface potentials yields inaccurate results. The inaccuracies arise because the transfer matrix relating epicardial and body-surface potentials is highly ill-conditioned, causing the inverse problem to be ill-posed. This means that the solution does not depend continuously on the data: small errors in the measurement of body-surface potentials and from the discretization of the geometry cause unbounded errors in the recovered epicardial potential data. Restoring the continuous dependence of the recovered epicardial potentials on the input body-surface potentials requires regularization techniques. While there exist several regularization schemes, all depend on a single error parameter - even though it is known that there is more than a single source of error, and that these errors are not equal in magnitude. This apparent weakness may lead to a reduction in the accuracy of the inverse procedure resulting from an over- or underestimation of the regularization parameter. Investigating the effects of single versus multiple error terms in a regularization scheme will allow us to accomplish the overall goal of improving the spatial resolution of the inverse solution.

The emphasis of this proposal is to establish, given current methodologies - and our improvements on these - the limits of spatial resolution of the inverse procedure using a realistic computer model. The short term significance of the proposed work lies in the development of better numerical and computational methods with which to calculate inverse solutions together with an improvement in our understanding of the effects of anisotropies and inhomogeneities on the inverse procedure as well as on the flow of current through the volume conductor. The long term significance is the anticipated realization of the utility of the inverse procedure for clinically assessing the electrophysiological state of the pathological heart in a noninvasive way.

Background specific to geometrical considerations of the inverse procedure includes the early models of Barr [11] and Rudy [3] utilizing concentric (or eccentric) spheres, and more elaborate models utilized recently by many investigators, including Colli-Franzone [6], Gulrajani [5], Johnson [8,14-16, see Appendix], Horacek [17], MacLeod [18-20], and Vahid [21], which employ realistic geometry reconstructed from fiberglass casts, magnetic resonance images (MRI), or CAT scans. These studies have focussed attention on the ability of the inverse procedure to recover epicardial potentials from a single, given geometry. More specific studies have been completed by Huiskamp and van Oosterom [1], who, using multiple realistic models, showed that the accuracy of their inverse solution was directly and sensitively dependent on the accuracy of the geometry and the position of the heart within the torso. Measures of error due to heart placement have also be reported by Rudy [2,3]. All of the more recent models have been discretized using either surface elements, primarily triangles (for use with the boundary element method), with the highest resolution of 3000 nodes with a spatial seperation of greater than 2.5 cm. [5]; or volume elements, primarily tetrahedra (for use with the finite element method), with the highest resolution (not including our latest models, introduced in the next section) of approximately 12,000 nodes and 72,000 elements with a spatial seperation of greater than 2 cm. between nodes[21]. To date, there has not been any specific published research which measures the level of spatial accuracy of the inverse problem in terms of the spatial resolution of the reconstructed geometry. The lack of researched results in this area provides the rationale for the proposed studies to perform simulations which measure changes in solution accuracy as a function of reconstructed geometrical accuracy.

Background material for the inclusion of anisotropy into the volume conductor for the inverse procedure is much more sparse in the literature. Representations of anisotropy have been treated generally in one of two ways; by extending the boundary and setting isotropic conductivities [5], or by representing the anisotropy by a conductivity tensor [8,14-16, see Appendix]. In the boundary extension method (primarily used with the boundary element techniques), the outer

boundary of the torso is enlarged by a factor dependent on the degree of anisotropy in order to replace symmetric anisotropic regions with an isotropic region of extended proportion. The major drawback of this method is that it can be used only within highly symmetric anisotropic regions and cannot represent continually changing directional regions such as those that occur within the skeletal muscle. Certainly one question which is prompted by this previous work is how much of the directional change of the anisotropic skeletal muscle needs to be characterized for an accurate inverse solution. Recently, it has been shown by Johnson [8,14-16, see Appendix] that inclusion of true directional anisotropy via conductivity tensors affects the accuracy of inverse procedure. It is this work which forms the rationale for further studies involving quantitative measures of the inclusion of directional anisotropy in a geometrically realistic way. As part of this project we will compare, quantitatively, the use of boundary extension versus assignment of individual conductivity tensors under otherwise identical conditions.

Background pertaining to the regularization of the inverse procedure involves a small set of studies by a few investigators. Successful regularization depends, first, upon the particular regularization scheme - singular value decomposition, generalized least squares, Twomey, or one of the Tikhonov methods - and, secondly, on the method of obtaining or estimating the *a priori* information necessary for constraining the solution or estimating the optimal regularization parameter. The most comprehensive to date has been the volumous work of Colli-Franzone [6]. Colli-Franzone thoroughly tested known regularization techniques, and concluded that those based upon the Tikhonov regularization scheme were superior. Colli-Franzone also produced a new method, CRESO, for determining the *a priori* regularization parameter. Most recently, a regularization scheme has been developed by Oster and Rudy [22]; this technique involves using the continuity in time of the cardiac activation process to apply the epicardial potential distributions from adjacent time frames in a Twomey procedure as a further constraint. Johnson [8,14-16, see Appendix] has introduced the concept of using multiple weighted error sources to develop a more accurate regularization process and to choose an order optimal regularization parameter. Furthermore, Johnson [8] has proposed that volumetric potential and potential gradient information be employed as a technique with which to further localize ectopic foci and onset of arrhythmia. Primarily because such a short amount of time has passed since the first application of these new techniques to problems in electrocardiography, there has not been any published research which documents comprehensive comparisons of these techniques, or combinations of techniques, in an adequately controlled way. The fact that regularization is such an important aspect of the inverse procedure and the small amount of new research into the mathematical properties of the regularization procedure as it pertains directly to the inverse problem in electrocardiography provide the rationale for further studies.

C. PRELIMINARY STUDIES/ PROGRESS REPORT

Pilot studies involving experiments, model construction, and computer simulations suggest both the necessity and the feasibility of the projects in this new proposal. While most such efforts have ignored some aspects of the complexity of this problem, our most recent work [14-16, see Appendix] indicates that inclusion of anisotropic inhomogeneity, higher geometric resolution, and improved regularization techniques could enhance - and may be necessary for - a spatially accurate noninvasive recovery of epicardial potentials.

We have developed a multi-component geometric model which is the computational equivalent of an electrolytic torso tank. Custom built in the shape and size of a child's torso, the torso tank provides a unique opportunity to validate forward and inverse problems in a tightly controlled enviornment (see color plates, figure 1-3, in Appendix). It is possible to insert current generators as simple as a pair of current electrodes and as complex as a perfused dog heart into the tank and measure the potential distributions on or near the surface of the source, throughout the tank

20

volume, and at the outer boundary. This tank, and the data recorded from it, were used to develop and test complete forward and inverse solutions and will be further employed to test our hypotheses.

Besides being able to perform forward and inverse simulations and validate them experimentally via the torso tank, we also have the unique ability to compare directly the boundary element method and the finite element method for the same experimental and computational conditions [8,14-16,18-20, see Appendix]. This will allow us to test thoroughly the accuracy of the two methods for a variety of situations, in particular since we model anisotropic inhomogeneities and employ models with different spatial geometry and resolution.

The first computational model that has been developed for solving the forward/inverse problem consists of a set of programs: 1) a three dimensional finite element program to solve the electrocardiographic field equation in its most general form (i.e. fully capable of handling anisotropic inhomogeneities as well as modeled current sources, boundary current sources, etc.), 2) an algorithm with which we can apply a general set of boundary conditions for use with various experimental and simulation conditions, and 3) a local Tikhonov regularization scheme, which constrains the solution and restores continuous dependence of the solution on the data. The latter is achieved by utilizing a generalized discrepancy principle which makes use of the measurement errors of torso potentials together with discretization errors to optimize the choice of the regularization parameter [14-16, see Appendix].

This computational model has been tested and validated using theoretical studies involving simplified geometries and in experimental studies utilizing the electrolytic torso tank. In the first studies, simulations were performed to validate the computational sequence and test the accuracy of the finite element program. These simulations were performed on a model of concentric spheres, where the innermost sphere represented the epicardial surface, the outer sphere represented the torso surface, and two internal spheres defined subregions of the volume conductor. When either a homogeneous or an inhomogeneous isotropic volume conductor was used, the outcome of the simulations could be compared directly with analytical results, thus allowing for unbiased, quantitative measures of solution accuracy. Forward calculations yielded %RMS (percent root mean square) errors of less than 2% RMS and inverse calculations yielded errors of less than 4% RMS, the primary source of error being attributable to the discretization of the geometry. Further simulations were carried out on the concentric spheres model using a nonsymmetric, anisotropic, inhomogeneous volume conductor. Here, the forward solution showed an error of 3% RMS while the inverse calculations incurred errors of 5% RMS [8,14-16, see Appendix].

Once the algorithms had been tested and validated on the idealized geometry, a series of experiments were carried out using the electrolytic torso tank. Initially, a forward solution was computed and applied to potentials recorded near the source (epicardial); the resulting estimated tank surface (torso) potentials (see color plates, figure 3, in Appendix) then formed the input data for an inverse solution using the same geometry. The predicted epicardial potentials were within 23% RMS of the experimentally recorded values, the major error being differences in amplitude. In another set of simulations, anisotropic inhomogeneities were introduced into the computational model and a second set of torso (forward solution) and epicardial (inverse solutions) potentials were computed. Comparison of the epicardial distributions from both simulations showed a further 10% RMS error when the anisotropic inhomogeneities where not accounted for; errors in this case included both a shift and a change in shape of the maxima and minima in the distribution [8,14-16, see Appendix]. *These studies suggest two relevant conclusions: that a multi-component model that includes anisotropic inhomogeneities and employs the finite element method can be constructed and used to recover epicardial potentials, and that by neglecting the anisotropic nature of these inhomogeneities, intolerable errors, especially with regard to the location and shape of the extrema, could be induced.*

A second computational model that has been developed is based on the boundary element method for solving Laplace's equation. In this formulation, the solution is defined by the relationships between the bounding surfaces of the geometry; hence, descriptions of the model geometry need only consist of node points and (typically) triangle connectivities, with no explicit knowledge of the volumes which these surfaces enclose. We have developed a boundary-element solution to the forward and inverse problems and used it to investigate the changes in epicardial potentials which arise during the acute, transient ischemia induced by cardiac balloon angioplasty [18-20, see Appendix].

The geometric model for studies conducted to date was derived from the Horacek torso [17] and consists of 352 node points and 700 triangles on the body surface and 92 nodes and 192 triangles on the epicardium and is shown in figure 8 in the Appendix. This model boasts a differential spatial resolution with internodal separations of approximately 2.5 cm in the precordial region and 5 cm elsewhere on the thorax, yielding a considerable reduction in computational complexity. A forward solution relating epicardial to torso potentials on this homogeneous model was computed and tested against direct calculations of potentials from single, stationary dipole sources. These same direct results then formed the optimization criteria for the regularization parameter in the inverse solution, which was computed according to the method of Tikhonov [23]. Several different types of Tikhonov constraining matrices were compared and a discrete Laplacian operator was found to outperform both identity and gradient matrices. Epicardial potentials recovered with this inverse solution differed from those computed directly from dipole sources by an average of 20% RMS error [20] (see section D for definition of %RMS error).

In order to evaluate qualitatively this inverse solution under more complex circumstances, body surface maps were recorded using signals from 117 locations on the anterior and posterior surfaces of the thorax before, during, and after inflations of a catheter balloon during percutaneous transluminal coronary angioplasty (PTCA). Difference maps made by subtracting pre-inflation from peak-inflation data were then multiplied by the inverse-solution matrix to estimate the changes in epicardial potential distributions associated with this regional ischemia. The location of ischemia in the resulting epicardial difference map was compared to the region of expected ischemia determined from angiographic examination of each patient during PTCA. While it is impossible to evaluate such results quantitatively, strong qualitative agreement between the areas of ischemia predicted by the two very different methods was found for occlusions of all three major coronary arteries. There were, however, regions of less pronounced ischemia predicted by the inverse solution which did not match those expected from the hemodynamic state of the patient (see figure 9 in Appendix and [20]).

The conclusions from these studies relevant to the present application are that:
1) the boundary element method is an adequate basis for forward/inverse solutions when the volume conductor can be approximated as homogeneous, or piecewise homogeneous;
2) although it is possible to detect the presence and approximate location of acute ischemia in humans using an inverse procedure implemented in a relatively simple model of the human torso, there are parameters which must still be optimized before such a procedure can be dependably used to evaluate completely the distribution of epicardial potentials;
3) controlled experiments using known sources and volume conductors that include inhomogeneities are necessary to evaluate quantitatively the spatial accuracy of the epicardial potentials predicted by an inverse solution.

One logical extension of these studies is to derive a geometric model based on actual human torso shape, including inhomogeneous regions and, where appropriate, their anisotropic nature. To this end, we have performed complete thoracic MRI scans on several subjects and, from one of these subjects, we have constructed two geometric models of different resolution (see color plates, figures 4-7, in Appendix). Conductivities have been assigned to each individual volume element in each model based on values from the literature [24,25]. These models form the basis for a set of

forward and inverse simulations in which we will examine the effects on the recovered body surface and epicardial potentials of: varying magnitude and directional dependence of the conductivities; the spatial resolution of the geometric construction; and *a priori* estimates of the regularization parameter.

Results which we have achieved pertaining to these models to date include:

1) Completion of the two most detailed torso models yet constructed for this purpose, consisting of, in one case, approximately 82,000 node points and 500,000 tetrahedral volume elements (high resolution), and, in the other, approximately 26,000 nodes and 150,000 tetrahedra (medium resolution). Figure 7 in the Appendix shows the torso, lungs and epicardial surface of the high-resolution model.

2) Individual surface representations of the body surface, subcutaneous fat layer, skeletal muscle layer, lungs, and epicardium for both models, and the development of tools to allow further additions and repetitions at different spatial resolutions. In figure 5 of the appendix is a photo of a single slice including torso, fat, muscle, lung, and epicardial surfaces from the MRI slice shown above it in figure 4.

3) Representation of the different electrically conductive tissues, including an algorithmic method for assigning anisotropy to skeletal muscle elements. Figure 6 in the Appendix shows a sample slice from the high-resolution model after it has be tetrahedralized and color-coded according to conductivity.

4) A method for interpolating 64-lead epicardial porential maps over the entire model heart surface.

D. DESIGN AND METHODS

Experimental Design and Protocols

The technology and methodology for many of the the experimental studies described in this application have been developed previously by the applicants and other investigators in our lab. While we will tap the wealth of previously collected data from animal and human experiments, we do intend to carry out specific torso-tank experiments and computer simulations designed to answer questions related to our hypotheses. In this section we describe the experimental methodologies necessary to carry out these studies.

Torso Tank

Of central importance in validating the modeling studies we propose are experiments to be performed in the controlled environment of an electrolytic torso tank that exhibits realistic geometry. The tank was designed by Drs. Bruno Taccardi and P.R. Ershler and Mr. B. Steadman at the Nora Eccles Harrison Cardiovascular Research and Training Institute (CVRTI). The tank consists of 1302 electrodes, of which 384 reside on the torso surface, 180 are positioned just outside the epicardial surface, and the remaining 738 fill the volume between the surfaces as shown in the photograph in Figure 1 in the Appendix. The torso electrodes remain fixed while the remaining electrodes are on retractable rods that are moveable within the volume to conform to specific heart and/or simulation geometries. An isotonic NaCl (46 mM) and sucrose (280 mM) solution with a resistivity of approximately 200 ohm cm fills the tank. Potentials from the tank are recorded using a 192-channel multiplexer and each signal is amplified and filtered to a bandwidth of 0.03 Hz to 500 Hz. Each amplifier is followed by a sample and hold circuit to insure virtually simultaneous sampling over all channels. After multiplexing, the data is converted in real time to

23

12–bit digital words by linear analog to digital converters. The data are sampled at 1 kHz and stored first in dynamic memory and then moved with DMA transfers to a hard disk drive on a Digital Equipment Corporation (DEC) Micro Vax II computer. Data is then transferred to a DEC VAX 11/750 for processing and display. To accommodate the large number of recording sites in the tank, the data are recorded in multiple banks of 192 leads, and the minimum time required between bank switches, 30-40 s, is determined by the rate with which data moves from memory to disk. Five reference leads are recorded in common with all banks to facilitate the time alignment of the individual banks of data during processing and to monitor stability of the signals over time.

In order to evaluate experimentally the effect of inhomogeneous - especially anisotropic inhomogeneous - regions in the thorax on the distribution of potentials and currents, it is necessary to add materials with appropriate conductivities to the torso tank. We will construct artificial "lungs," "fat," and "muscle" inserts from materials with conductivities which approximate physiological values [25]. To produce the anisotropic effect of skeletal muscle, we will use hollow silicon fibers, similar to those used in oxygenators such as CardioPulmonic's IVOX. Once the fibers have been effectively grouped and shaped to represent striated muscle tissue, an ionic solution will be added to achieve the desired conductivity.

The electric sources for the torso tank will consist of discrete sources and isolated dog hearts. The discrete sources will be modeled by configurations of current sources and sinks, which can be placed at any desired location within the tank volume and driven with time-varying signals. We will also use data from animal experiments performed by Dr. Bruno Taccardi, as part of his studies into the nature of three-dimensional propagation in the heart and according to protocols which have been approved by the University of Utah Institutional Animal Care and Use Committee: two pentobarbital anesthetized dogs will be used in a modified Langendorff preparation for each such experiment. One of the dogs will support the circulation of the isolated heart to be studied. The isolated, perfused heart will be first fitted with a multi-electrode sock (see epicardial mapping methods, below) and then suspended in the tank at a location and orientation approximately equivalent to that of a human heart.

Epicardial Potential Mapping

Recording of epicardial potentials can be carried out both in experimental studies in animals [26-29] as well as for clinical purposes on humans [30]. The technology in both cases is essentially the same, based on multiple individual wire electrodes mounted in an elastic sock or band that is slipped around the heart.

Electrode arrays: All electrode sock arrays are fabricated at the CVRTI from nylon stocking material tailored to fit a plaster cast of a heart. The electrodes are formed from .125 mm diameter enamel insulated silver wire which is stripped at the tip and knotted to the stocking at locations indicated on the plaster cast, forming very fine unipolar electrodes. The other ends of the wires are stripped and soldered to connectors.

Experimental mapping: In animal experiments, stimulating electrodes will first be sutured to the right and left ventricle of the isolated heart and then a 64-lead nylon sock will be slipped over both ventricles. In experiments from which we will determine spatial resolution of the inverse solution, a row of closely-spaced electrodes will be used to mimic stimulation from multiple sites.

Clinical epicardial mapping: After body surface potentials mapping has been performed and the chest has been surgically opened, but prior to the necessary heart surgery (such as ablation of the Kent bundle in Wolff-Parkinson-White syndrome or localization and disruption of reentrant loops in ventricular tachycardia), a 64 electrode recording array is placed on the heart. Samples of data are recorded during sinus rhythm and then again when the arrhythmia has been induced by

programmed stimulation. These data will be gathered primarily for clinical diagnostic purposes and are supplied to us by Dr. L. Green as part of an existing clinical protocol [30].

Data acquisition: Data is recorded using a multiplexer consisting of 64 or 192 low noise, high input-impedance instrumentation amplifiers. Each of the unipolar amplifiers is referenced to a Wilson Central Terminal. Each amplifier incorporates a sample and hold circuit to insure simultaneous sampling. Data is sampled at 1000 samples per second per channel and digitized using a 12-bit linear analog to digital converter. Two to fifteen seconds of data are recorded and stored on hard disk for later offline processing.

Data Processing: During processing, the signals are gain adjusted and corrected for baseline drift. The data from multiple cardiac cycles can be averaged to reduce noise and minimize effects of beat-to-beat variations. Isopotential maps from a single sample instant are typically constructed every 5 ms during the QRS interval and every 20 ms during the ST-T interval, although data are available for every millisecond during the entire QRST interval.

Epicardial signals are recorded at only 64 locations but must be interpolated to all the nodes of the model epicardium before they can be used to drive a forward solution. This involves first matching the electrode locations with the nearest node location and then interpolating over the entire surface to generate potentials values for all other nodes. The interpolation is performed using a method described by Oostendorp *et al.* in which the discrete Laplacian for the potential distribution over the epicardial surface is minimized [31].

Magnetic Resonance Imaging

Accurate rendition of the geometry to which the forward and inverse solutions are applied is required in order to approach the questions of spatial resolution and the effect of anisotropic inhomogeneities. The most exact method of performing three-dimensional reconstruction in humans, without subjecting them to unacceptable radiation, is by means of magnetic resonance imaging techniques. To this end the assistance and co-operation of the MRI facilities of both the the LDS Hospital and University of Utah Medical Center has been secured previously for this work.

In order to achieve the 1-cm resolution in inverse calculations of potentials on the epicardial surface, we perform all MRI imaging at a slice step of 5 mm. Sampling of the patient is performed using a Signa 7 imaging system (General Electric Corp.) and a Data General computer; the scan extends from just below the umbilicus to just below the chin (typically 60-70 cm) and requires approximately 60-90 minutes to complete. Before beginning the tomography, a set of 192 mineral oil-filled phantom electrodes are applied to the subject according to the standard procedure for 192-lead body surface mapping (see next section). Mineral oil appears opaque in MRI images and can be used to locate the electrode positions. Data transfer between the MRI center and our lab occurs via industry-standard digital magnetic tape. An example of a single MRI slice which includes the heart, lungs, and muscle and fat layers is shown in figure 4 of the Appendix.

Body Surface Potential Mapping

Body surface potential mapping provides the input data for the inverse computations and is carried out according to several protocols which have been developed in our laboratory [35, 36]. The procedures differ only in the number and location of electrodes used and in the order and duration of recordings.

192-lead BSPM: In experimental mapping studies on humans, 192 electrodes are arranged in 16 vertical strips with 12 electrodes (5 cm interelectrode distance) in each, evenly spaced around the entire torso of the subject. Recording duration ranges from 5-15 s at a sampling rate of 1000 Hz.

32-lead BSPM: For mapping in the clinical environment, we use a mapping system which includes 32 electrodes located according to the reduced lead configuration devised in our laboratory [32,33]. Electrodes are arranged in an irregular grid at specific locations on the patient's anterior and left and right lateral thorax. The ability of this 32-lead electrode array to estimate 192-lead maps has been tested in a variety of patients with an average root-mean-square (rms) voltage error of only 35 μV and a correlation coefficient of 0.97 [32-34].

PTCA Recording Protocol: In order to evaluate the effect of acute transient ischemia on the distribution of body surface potentials, we have recorded body-surface maps from patients undergoing percutaneous transluminal coronary angioplasty [18-20, 37-38, see Appendix]. Individual recordings consisted of 15 s of continuously recorded data at a sample rate of 500 Hz. Such recordings were taken before the PTCA treatment was begun, then just before and during the last 15 seconds of each inflation of the angioplasty balloon. A second baseline recording was made after the balloon had been allowed to deflate.

Processing of BSPM Data: The processing of signals recorded from body surface potential mapping varies somewhat, depending on the nature and quality of the recording; in general, however, processing proceeds as follows:

Before processing, all clinical map recordings are converted, if necessary, into 192-lead samples, using the estimator developed in our laboratory [32, 33]. With an interactive computer program developed for this purpose [34, 36], five to fifteen consecutive complexes are selected and aligned by means of a cross-correlation analysis which compares the entire 5-20 second data sample with a manually selected, large amplitude QRS from the sample. The program then computes the average from the set of aligned beats, which is assumed to represent the stable electrical state of the heart. From the averaged beat for each location, isopotential and isointegral contour maps can be constructed. Isopotential maps are normally drawn at 5 ms intervals during the QRS and 10 ms intervals during the ST-T wave. Isointegral maps are normally computed by evaluating the area under the average ECG during the QRS, QRST, and ST segments.

For use in forward and inverse calculations, the measured body surface potentials must be interpolated in order to generate values for all nodes of the model body surface. The same procedure as was described for the epicardial potential maps is used for the body surface potentials.

Geometric Model Construction

While magnetic resonance tomographic images provide the basis for reconstruction of the geometry required for forward and inverse calculations, there is a great deal of manipulation required before it is available for computations. This processing consists of extracting, from the 100-140 slices of image data, the location and shape of the major surfaces within the thorax: body surface, subcutaneous fat, skeletal muscle, lungs, and epicardium. The volumes within each of these surfaces must then be discretized into tetrahedral elements and assigned realistic conductivity values. The surfaces themselves are also tessellated into triangular elements and used both for model computations and for subsequent graphical display of the results.

The output from the MRI system is stored in digital form on magnetic tape on site. These tapes are then transferred to a DEC VAX 750 computer and the data from each layer of the scan is placed in a single file. A local area computer network then carries these files to a MACINTOSH II computer on which they can be displayed and the surfaces manually digitized [39]. The sampled points ("raw layer data") from all the surfaces are stored in one file for each layer of the thorax. These

files are then transferred back to the DEC VAX 750 and a Silicon Graphics Iris 4D/210 VGX for further refinement.

In order to establish a uniform spacing of the points defining the surfaces, we interpolate the raw layer data using a parametric cubic-spline algorithm programmed for this application. The value of point separation set in the interpolation program depends on the complexity (curvature) of the individual layer being processed and typically ranges from 3 to 10 mm. As part of the interpolation process, the program also extracts the point co-ordinates from the individual surfaces and stores them in separate files. Hence, at this stage of the process, there are files containing the outlines of each surface in each layer returned from the MRI scan. Points from pairs of successive layers of the same surface are then combined into "slices"; that is, they represent volumes and not just planar layers. The points in these "slice-files" are then connected to form triangles which define the outer surface of the slice. We have written programs to perform this triangularization which use a local nearest-neighbor criteria to construct triangles that are as close to equilateral as possible. The triangulated slices occasionally require some manual editing, which we perform using a program written for an Evans and Sutherland, PS-390 graphical workstation. A sorting program then produces complete descriptions of each surface containing the points and triangle connectivities from all slices that contain points from that surface. Figure 5 in the Appendix shows a color reproduction of the single triangulated slice which was generated from the MRI image above it in figure 4. In figure 7 are shown the complete torso, heart and lung surfaces for the high-resolution model.

Calculations using the finite element method (FEM) require that the entire volume within the surfaces be tessellated into volume elements. We have chosen to use tetrahedral volume elements since they are capable of closely following the irregular geometry associated with the human body. The first step in terahedralization of the model is to add to each layer the node points that are the vertices of the elemental volumes. For this, we have devised a "grid-maker" that applies a uniform grid of points to the layer and then excludes those points which are outside the outer surface or too close to any surface in the layer. Once the grid points are defined, all the points from a single slice (two successive layers) are input to a program that connects sets of 4 nodes into volume elements based on three dimensional Delaunay and Dirichlet criteria for optimal tetrahedra [40, 41]. Figure 6 in the Appendix shows a single slice after it was tetrahedralized.

Torso Tank model: The shape and electrode locations of the torso tank are, of course, well defined and form the basis of model geometry. Figure 2 in the Appendix contains a photo of the triangulated model of the torso tank including the surface defined by the tips of the recording electrodes closest to the source (heart). The introduction of inhomogeneities into the tank, however, requires construction of new models using the same methods as those outlined for the construction of human models. We will fabricate the inserts for the torso tank based on normal human anatomy after appropriate scaling. The inserts will then be mounted on thin rods which will allow us to determine location and orientation once they are in place. It will then be possible to incorporate the inserts into the geometry of the torso tank and perform the same steps of triangularization and tetrahedralization as described above for the MRI-based models. The tools we have developed will allow for relatively simple re-discretization of the model so that the role of the accuracy and resolution of the model geometry in obtaining accurate inverse solutions can be determined.

Model resolution: Since it is our intention to develop a solution to the inverse problem capable of resolving cardiac electrical activity down to the order of 1 cm, we have based our MRI scanning and subsequent model construction on a similar scale.

A model of the torso tank has already been constructed using the locations of the electrodes on the tank inner surface and electrodes mounted in the rods as the only node points (see color plates, figure 2, in the Appendix) . Such a model yields approximately 1300 nodes and 8000 tetrahedra

and contains no inhomogeneities. We will construct several new models of the tank, using the methods already described, at resolutions of 5, 10, and 15 mm; these models will include the inhomogeneities and their anisotropic nature.

In the geometric models based on human MRI images, we have obtained the following configurations for the high (H) and medium (M) resolution versions:

Surface	# Surface Nodes (H/M)	# triangles (H/M)	Totals	# Elements (H/M)
Torso	12,000/3,000	24,000/5,700	Surface nodes	42,400/10,550
Fat	11,900/2,600	23,600/5,150	Grid nodes	39,600/15,450
Muscle	11,700/2,400	23,200/4,700	Total nodes	82,000/26,000
Lung	5,500/1,250	11,000/2,325	Triangles	84,450/19,525
Epicardial	1,300/1,300	2,650/2,650	Tetrahedra	500,000/150,000

To compute forward and inverse solutions with the high resolution version of such a model using the finite element method would require an estimated three days of CPU time and 8 GByte of storage on an IBM 3090 supercomputer using our original algorithms. Initial steps towards optimization of these programs have already resulted in a 33% reduction in expected compute time from these estimates. While the medium resolution model contains considerably fewer elements than the high resolution version, it is still twice as large as any other thorax model reported in the literature. We will use these, and a series of other models based on the same original data, to test and improve our algorithms and to determine the relationship between the spatial resolution of different model geometries and the accuracy of the inverse solutions they produce.

Assignment of conductivity: The major advantage of the finite element method is the ability to assign local conductivity information to each element of the volume. Hence, it is also possible to include the effect of anisotropy in a finite element solution. In figure 6 in the Appendix is depicted a single slice of the high-resolution model after it was tetrahedralized and color-coded according to conductivity values.

In the torso-tank experiments we intend to perform, we will include materials of known conductivities, some isotropic and others with considerable anisotropy. Since the shape of these inserts in the tank is well known, it will be a simple matter to assign the appropriate conductivities to the equivalent elements in the model. The silicon fibers we will use to mimic anisotropic skeletal muscle even allow the conductivity to be controlled via the ionic solution with which they are filled, thus we will be able to vary experimentally the anisotropic conductivity of a defined region of the volume conductor and observe the effects on forward and inverse solutions.

For calculations with the models based on human data, we will utilize data from the literature to assign conductivities to the fat, muscle, and lung regions [25]. We will determine the direction of the skeletal muscle fibers algorithmically based on the location of the volume element in the model according to anatomical data in the literature [24].

Mathematical Theory

The electrical activity due to cardiac sources is governed by Maxwell's equations. It has been shown that we can neglect capacitive, inductive, and electromagnetic propagation effects [42]. The electrocardiographic field equation is thus expressed as a generalized Poisson equation,

$$-\nabla \cdot (\sigma \nabla \Phi) = I_{SV} \qquad in \quad \Omega \qquad (1)$$

where:

Φ = Potential field defined in Ω

Ω = Bounded domain

σ = Conductivity tensor

I_{SV} = Internal current source per unit volume

The general inverse problem in electrocardiography is considered by solving the quasi-static formulation of (1) which assumes that steady-state conditions throughout the volume conductor are established instantaneously. This requires the solution of (1) with the boundary conditions:

$$\Phi = \Phi_0 \qquad on \quad \Sigma \subseteq \Gamma_T \qquad (2)$$

$$(\sigma \nabla \Phi) \cdot \vec{n} - \vec{g} = 0 \qquad on \quad \Gamma_T \qquad (3)$$

where:

Φ_0 = Potentials on the boundary (known *a priori*)

$\vec{g}$ = Externally applied boundary current (if one exists)

$\vec{n}$ = Unit normal vectors

Γ_T = Boundary at torso surface

Σ = Subset of torso boundary

Of particular relevence to this study is the solution of (1-3) in terms of potentials, specifically the solution of epicardial potentials in terms of torso potentials. This has the advantage over other formulations, [43, 44] in that the solution is unique. Furthermore, it has been shown that epicardial potentials accurately represent the electrical activity of the underlying myocardium [3,49]. This leads to a particular formulation of (1-3) which requires $I_{SV} = g = 0$. [Note: for a full description of the mathematical derivations, see the appendix.]

Finite element solution: When the finite element method is used to discretize the solution domain, the set of equations to be solved reduces to a system of linear algebraic equations:

$$\sum_{e=1}^{E} K_{ba}^{e} \Phi_a = 0 \qquad (4)$$

,

with $\Phi = \Phi_0$ on $\Sigma \subseteq \Gamma_1$ and $(\sigma_{ij} \nabla \Phi) \cdot \vec{n_i} = 0$ (on the body-surface), which are the Dirichlet and Neumann boundary conditions, respectively. Here the matrix K contains all the geometric and conductivity information of the problem. The latter is in the form of a three by three conductivity tensor for each element that represents specific tissue conductivities within the

29

inhomogeneous torso. The matrix relationship between the epicardial and torso potentials can be formulated in terms of the partitioned K matrix, which contains local geometric and conductivity information,

$$\Phi_E = (K_{TV} K_{VV}^{-1} K_{VE} - K_{TE})^{-1} (K_{TT} - K_{TV} K_{VV}^{-1} K_{VT}) \Phi_T, \qquad (5)$$

where subscripts T, V, and E stand for the nodes in the torso, volume, and epicardial regions, respectively.

The equation 5 can be expressed more concisely by combining all of the K submatrices into a single transfer matrix as:

$$\Phi_E = A_{TE}^{-1} \Phi_T. \qquad (6)$$

Boundary Element method: The boundary element solution method may also be applied to this problem, starting form the same equation (1) with boundary conditions expressed as in equations (2) and (3). We may use Green's second identity and the boundary conditions to write for body-surface potential ϕ_T and epicardial potential ϕ_E,

$$\phi_T^i = \frac{1}{2\pi} \int_{S_E} \phi_E d\Omega_{TE}^i - \frac{1}{2\pi} \int_{S_T} \phi_T d\Omega_{TT}^i - \frac{1}{2\pi} \int_{S_E} \nabla\phi_E r_i^{-1} \cdot d\vec{A} \qquad (7)$$

$$\phi_E^i = \frac{1}{2\pi} \int_{S_E} \phi_E d\Omega_{EE}^i - \frac{1}{2\pi} \int_{S_T} \phi_T d\Omega_{ET}^i - \frac{1}{2\pi} \int_{S_E} \nabla\phi_E r_i^{-1} \cdot d\vec{A} \qquad (8)$$

where the superscript i indicates the location of a point on the surface, and the Ω terms are solid angles. In order to solve these equations for an arbitrary surface, we can discretize them, converting the integrals to summations, and derive a system of linear equations. This system can then be reduced to a single equation relating the epicardial and torso potentials directly:

$$\Phi_T = A_{TE} \Phi_E \qquad (9)$$

This matrix is identical to that found using the finite element method for the case of a homogeneous volume conductor and represents the *forward solution* to this problem. To derive the *inverse solution* from this the same methods can be used, independent of how the forward solution was calculated.

Inverse solution: To compute the epicardial potentials from body surface potentials it is necessary to invert the transfer matrix A_{TE} derived above in equations 6 and 9,

$$\Phi_T = A_{TE} \Phi_E$$

Here $\Phi_T \in \phi_T$, $\Phi_E \in \phi_E$ and $D \subset \phi_E$. ϕ_E and ϕ_T are chosen as Hilbert spaces and D is the set of

a priori constraints. A_{TE} is assumed to be a linear one-to-one operator from ϕ_E to ϕ_T. Inversion of the transfer matrix leads to a problem that is ill-posed in the Hadamard sense [45]. The methods utilized here to restore continuity of the solution onto the data involve the class of Tikhonov regularizers [23].

The error between the approximate data and the true data is represented by an error vector:

$$\varepsilon = \{\delta_1, \delta_2, \ldots, \delta_n\} \tag{10}$$

One wishes to find, using approximate data, a vector $\Phi_{E\varepsilon} \in D$ such that $\Phi_{E\varepsilon} \to \Phi_E$ as $\varepsilon \to 0$. The two largest sources of error are those due to discretization of the volume conductor, $\|\widetilde{A}_{TE} - A_{TE}\| \leq \delta_1$, and errors in measuring the torso potentials, $\|\widetilde{\Phi}_T - \Phi_T\| \leq \delta_2$. We can find $\Phi_{E\varepsilon}^{\alpha}$ by minimizing a generalized form of the Tikhonov:

$$M^{\alpha}\left[\Phi_E, \widetilde{\Phi}_T, \widetilde{A}_{TE}\right] = \|\widetilde{A}_{TE}\,\Phi_E - \widetilde{\Phi}_T\|_{\phi_T}^2 + \alpha\,\|C(\Phi_E - \Phi'_E)\|_{\phi_E}^2 \quad \alpha > 0 \tag{11}$$

in terms of the epicardial potentials,

$$\Phi_{E\varepsilon}^{\alpha} = [(\widetilde{A}_{TE})^T\,\widetilde{A}_{TE} + \alpha C^T C]^{-1}\,[(\widetilde{A}_{TE})^T\,\widetilde{\Phi}_T + \alpha C^T C\Phi'_E)] \tag{12}$$

where $\Phi_{E\varepsilon}^{\alpha}$ is the estimate of the epicardial potentials dependent on the regularization parameter α and on the error vector ε, $\widetilde{A}_{TE}$ is the approximation of the true transformation matrix A_{TE}, $\widetilde{\Phi}_T$ are the measured torso potential values, Φ'_E are *a priori* constraints placed on the epicardial potentials, and C is a constraint matrix. Note: The superscribed T stands for the matrix transpose (distinct from the subscripted T which signifies torso). Typical constraint matrices include the identity matrix and the first and second order spatial differential operators. The regularization parameter is found by utilizing a discrepancy principle [8, see Appendix] which minimizes the *a priori* estimate of the error vector ε.

Quantization of Simulation Results

Central in all of the aims of this project is to evaluate *quantitatively* the performance of the forward and inverse solutions. The use of the realistically shaped torso tank allows for a great deal of control over all aspects of the experimental studies, the results of which will serve as the "gold standard" for our simulations. What follows is a description of the ways this control will be maintained in comparing the simulations with recorded data.

Accuracy of potential distributions: Both the forward and inverse solutions yield results in terms of potential values at the node points of the surfaces of the model. The following statistical measures of agreement will be used to compare calculated and measured potential distributions:

Root-Mean-Squared (RMS) difference, defined as:

$$\left(\frac{\sum\limits_{i=1}^{N} (\Phi_i^C - \Phi_i^M)^2}{N} \right)^{\frac{1}{2}},$$

where Φ_i^C are the calculated potentials and Φ_i^M are the measured values. The value of the RMS difference is given in the absolute units of potential difference.

Percent RMS error (%RMS), which is simply the RMS error normalized by the RMS value of the measured distribution, in defined as:

$$\left(\frac{\sum\limits_{i=1}^{N} (\Phi_i^C - \Phi_i^M)^2}{\sum\limits_{i=1}^{N} \Phi_i^M} \right)^{\frac{1}{2}}.$$

The smaller the value of either %RMS or the RMS difference, the closer the two distributions are to being identical.

For the Correlation Coefficient, each set of potentials is viewed as a vector in N-space and the "angle" between them is calculated as a scalar product of the two vectors, normalized by the product of the respective magnitudes. For the computed and measured potentials, this can be written as

$$\frac{\overrightarrow{\Phi^C} \cdot \overrightarrow{\Phi^M}}{\left| \overrightarrow{\Phi^C} \right| \left| \overrightarrow{\Phi^M} \right|}.$$

Values of the correlation coefficient approaching 1 indicate a close match between the two vectors, and therefore, similar potential distributions.

Measures of resolution: One measure of local spatial resolution is the degree to which two discrete events can be recognized as separate on the epicardial surface. Experimentally, we will produce 'epicardial' and 'body-surface' (tank surface) distributions from discrete bipolar sources at variable separations. We expect the potentials from these sources to merge into a single maximum or minimum on the torso surface but that the inversely calculated epicardial distributions will reveal the discrete nature of the source. The distance between the two sources at which we can just distinguish them as separate in computed epicardial distributions will be used as a measure of local spatial resolution.

A second measure of spatial resolution is the absolute ability of the inverse solution to localize a discrete electrical event on a surface. By simulating such discrete events using single of multiple bipolar sources in the torso tank, we will be able to record potentials at the 'epicardial' surface and compare them to computed distributions. Measured 'epicardial' potentials should contain a localized maximum near one pole and a complementary minimum near the other. The distance on the 'epicardial' surface between the location of a particular measured maximum or minimum and

the location of the same feature as predicted by inverse calculations will serve as a measure of the absolute error of localization.

In both of the above cases, distances between locations on a three-dimensional surface must be calculated. We will not use any simplifying and distorting projections of such points to a plane, but instead will track the distance between points over the triangularized surfaces of the model.

Experimental and Computational Studies / Timetable

The specific studies we intend to perform, and their relevance to the hypotheses of this study are described below within the framework of the schedule.

Year 1 - Torso Tank based Forward and Inverse Solutions with Discrete Sources

Construction of anisotropic inhomogeneous inserts: based on the internal surface descriptions gleaned from the high resolution model of the human torso, we will construct inserts that will mimic the passive electrical characteristics of inhomogeneous and anisotropic elements of the thorax. These inserts will be developed from materials that will provide control of conductivity and the degree of anisotropy.

Development of computer models based upon inhomogeneous inserts: New geometric models of the torso tank at different resolutions will be constructed that will allow easy inclusion of the inhomogeneous inserts. Planned are models at 5, 10, 15, and 20 mm mean node separation.

Tank experiments with discrete sources: We will construct single and multipole source models which will be encased in a heart-shaped cast over which an epicardial sock can be placed. The location, orientation, and driving current for these sources will be determined from reports on discrete-source inverse models described in the literature in order to produce realistic potentials at the 'epicardial' and 'torso' locations in the torso tank. Epicardial potentials will be recorded using a 64-lead epicardial sock slipped over the heart cast and the inhomogeneous inserts will be added and removed from the tank. The effect of these inserts will be documented by means of torso surface potential distributions and quantified statistically. We expect the potential distributions on the tank surface to be shifted spatially and altered in amplitude due to the inclusion of (anisotropic) inhomogeneities.

Initial studies on the effect of geometric model resolution: Using the forward and inverse models developed from the torso tank geometry, we will evaluate the ability of the inverse solution to reproduce the measured epicardial potentials gathered in the discrete-source experiments. By comparing the results from the different geometric models, we will determine the dependence of recovery of epicardial potentials on the spatial resolution of the geometry. We expect that models constructed with smaller internode distances will outperform those sampled at lower resolution. What is more difficult to anticipate - and this is one of the specific goals of this project - is the degree of improvement that can be achieved as a function of the spatial resolution of the model.

Development of 3D graphical display: One of the most important tools for conducting such comparative studies with many different models is the ability to display the three-dimensional results in a realistic and flexible form. We will make use of the GL-graphics software common to all the IRIS graphics workstations of Silicon Graphics Inc. to develop a set of viewing and rendering tools for this project. The surface data associated with each geometric model provide the grids on which potentials distributions will be color-coded and rendered. Display algorithms for current data in the thoracic cavity will also be developed using some of the volume-viewing

routines of the apE [46] software from the Ohio Supercomputing Institute. The standard for all hard-copy from these programs will be the Postscript language from Adobe Systems.

Year 2 - Torso Tank based Forward and Inverse Solutions with Epicardial Sources

Experiments with perfused dog hearts: In the second year of the project, we will obtain data from experiments performed by Dr. B. Taccardi as part of his investigation into the three-dimensional excitation of the heart. In these experiments, the discrete source models will be replaced by perfused canine hearts. Epicardial potentials will be recorded using the 64-lead sock with the heart located at an anatomically correct position in the torso tank and with different combinations of the inhomogeneous inserts present in the tank. Various stimulation protocols will be used, including simultaneous stimulation from pairs of electrodes which are at separations of 5, 10, 15, and 20 mm. From the results of these experiments we will be able to measure the minimal separation at which dual stimuations can be resolved in the potential distributions on both the epicardial and torso tank surfaces. Areas of local ischemia will also be induced through either the transient occlusion of the left anterior descending artery or injection of formalin. It is expected that ischemic tissue will display altered excitability which will be visible on the epicardial surface but may not appear obviously on the torso tank surface, especially when inhomogeneities are inserted in the tank [49].

Continued studies on the effect of geometric model resolution: Using the data collected from the animal experiments in the torso tank, we will extend studies of the inverse solution to examine its ability to separate electrical activity at two closely spaced stimulation electrodes on the epicardial surface of the dog heart. We will compute epicardial maps for each pair of stimulation electrodes using the inverse solution based on each of the different (different spatial resolution) torso tank models. This will determine the limits of spatial resolution as a function of model resolution for the inverse solution.

Studies of the effect of inhomogeneities: The data from the animal experiments will then be compared, in both forward and inverse simulations, with computed results in order to measure the effect of inhomogeneities in the tank. Specifically, we will define the minimal spatial separation of simultaneous epicardial stimulation that can be resolved, both at the tank surface and from epicardial distributions generated by the inverse solution. The effect of the inhomogeneous inserts on the limits of resolution will be examined, first by using an inverse solution that includes these inserts and then with other solutions that include either none or some of them. We expect spatial resolution to be best when inserts are included in the model solution but cannot anticipate which of these inhomogeneities brings about the largest degradation of resolution when they are not included in the simulations.

Comparison of the boundary element method versus the finite element: Forward and inverse solutions based on the boundary element method will be developed for the homogeneous and piecewise inhomogeneous (and isotropic) volume conductor and compared with the solutions based on the finite element method. Specifically, we will examine the computational efficiency and accuracy of the predicted potential distributions under various configurations (with and without inhomogeneous inserts) of the torso tank for both methods and contrast their strengths and weaknesses for particular tasks. We expect the boundary element method to perform well under homogeneous conditions but to provide less accurate results when anisotropic inhomogeneities are present. We will also test the volume expansion method used by McFee and Rush [47] and Gulrajani [5] to account for the anisotropic nature of thoracic inhomogeneities.

Initial studies of regularization methods: We intend to generalize the mathematical formalism necessary to apply the weighted error technique to different regularization schemes, including all orders of Tikhonov methods and the Twomey method. From the torso-tank models it will be

possible to estimate the discretization error based on the measured discrepancy between forward calculated torso potentials and experimentally measured torso potentials. Different regularization schemes will also be compared according to their ability to recover epicardial potentials and localize discrete epicardial events.

Year 3 - Computer Model Based on Human Data - Forward Problem

Forward solutions using epicardial human data: In the third and fourth years of this project we will make use of the results of forward and inverse simulations and experiments from the torso tank to apply the forward solution to geometric models based entirely on data from human subjects. The intent of the initial work will be to quantify the effects of spatial resolution of the human model geometry and the role of realistic inhomogeneities on potential and current distributions. Models will be developed from MRI scans of a small set of patients on whom body su rface potential mapping and open-chest arrhythmia surgery will be subsequently performed. Wewill use MRI scans performed on patients according to existing protocols (Dr. L. Green) and with their informed consent.

Geometric model resolution: In order to evaluate the effect of geometry on the recovery of body-surface potentials, we will perform forward computations using geometric models of varying spatial resolution based entirely on human anatomical data. Epicardial potentials recorded from patients during open-chest surgery will be used to drive these simulations and the resulting body-surface potentials will be compared with body surface maps recorded from the same patients prior to surgery. These computations will be repeated for each of several different versions of the geometric models, at different resolution, and the effect of errors in model geometry on the resulting body surface distribution will be quantified.

Role of the anisotropic skeletal muscle: We will conduct forward simulations using models based on human anatomy in which the direction and strength of the anisotropic skeletal muscle layer will be varied. From potential gradients computed within the volume conductor, we will derive the current flow in the thorax and document the changes in current brought about by variations in anisotropy of the skeletal muscle.

Year 4 - Computer Model Based on Human Data - Inverse Problem

In the fourth year of the project, we will continue to use the geometric models based on human data to evaluate the accuracy and utility of the inverse solution methods developed from the torso tank studies.

Inverse solutions using human data: Inverse solutions driven by recorded body surface measurements will be used to estimate epicardial potential and isochrone distributions. The resulting isochrone maps will then be compared with those recorded during subsequent open-chest surgery on the same patients. As in the studies planned for year 3, we will vary the spatial resolution of the geometrical model and evaluate its effects on accuracy of the recovered epicardial potentials. Changes in anisotropy will also be applied to the inverse solution in order to evaluate its effect on the recovery of epicardial electrograms.

Role of geometry in the inverse solution: One of the key questions in determining the applicability of the inverse procedure in clinical electrocardiography is the degree to which the geometry of the volume conductor must be known to produce useful results. In studies which will span the final two years of the project, we will determine to what extent accurate epicardial potentials distributions and isochrone maps can be derived from body-surface potentials when the geometry of the actual patient is not available. Patients for whom complete sets of epicardial and body-surface potentials were recorded and MRI scans were performed will have inverse solutions

computed. The same potential data will then be applied to models which are based on different patients and the resulting error will be quantified. Our goal is to establish a set of torso models and the criteria which will allow us to apply them to other patients, along with a measure of the errors that such a procedure might involve.

Continued studies on regularization: During this time, we will also undertake theoretical studies involving the use of volumetric potentials and potential gradients to further constrain the choice of the regularization parameter. The possibility of using combined volumetric Tikhonov regularizers and temporal Twomey regularizers in constraining the inverse procedure will be explored.

Year 5 - Application of the Inverse Procedure in Human Subjects

The final year of the project is dedicated to the application of knowledge gleaned from previous phases of the work to selected problems in clinical electrophysiology.

Wolff-Parkinson-White (WPW) Syndrome: Body surface potential maps of patients about to undergo surgery for WPW syndrome will be used as input for the inverse solution which is based on a geometrical model either from the patient's actual anatomy or one closely matched in size and configuration. The location of pre-excitation will then be determined from computed epicardial maps. During surgery, epicardial maps will be recorded as part of the standard clinical procedure at the University of Utah Medical Center; these maps are used to assist in locating the aberrant atrioventricular conduction pathway. The surgically determined location will then be compared to that predicted by the inverse solution. Our goals in these studies is to be able to localize, given a geometrical model of sufficient accuracy, the site of pre-excitation to within 1-2 cm.

Percutaneous Transluminal Coronary Angioplasty: From preliminary studies (see section C), of acute, transient ischemia during inflation of the angioplasty catheter balloon, we know that body surface potential maps recorded during PTCA reveal evidence of underlying cardiac ischemia. In this study, we will attempt to demonstrate further localization of the site of ischemia using the inverse solution from body surface maps recorded before and during PTCA balloon inflation. We expect that by using more accurate, better discretized patient geometry and the advanced mathematical techniques we will have developed, that a more definitive epicardial distribution, without the spurious extrema found in earlier studies [18-20, see Appendix] will be observed.

E. HUMAN SUBJECTS

Not applicable

F. VERTEBRATE ANIMALS

Not applicable

G. CONSULTANTS

The validation of the computer simulations with data from controled experiments is an important part of the proposed research. Fortunately, Dr. Bruno Taccardi, a renowned authority on cardiac electrophysiology, has graciously consented to share data from his animal experiments including measurements of electrocardiographic potential distributions. Dr. Larry Green, a specialist in clinical electrocardiology, has consented to share data from his measurements of human torso geometry via MRI scans, and body surface and epicardial surface potential distributions. Note: letters of support can be found in the appendix.

H. CONSORTIUM/CONTRACTUAL AGREEMENTS

Not applicable

I. REFERENCES

(1) G. Huiskamp and A. van Oosterom, Tailored versus realistic geometry in the inverse problem of electrocariography. *IEEE Trans. Biomed. Eng.*, BME-36(8), pp. 827-835, 1989.

(2) B.J. Messinger-Rapport and Y. Rudy, Regularization of the inverse problem: a model study of the effects of geometry and conductivity parameters on the reconstruction of epicardial potentials. *IEEE Trans. Biomed. Eng.*, BME-33(7), 667, 1986.

(3) Y. Rudy, and R. Plonsey, A comparison of volume conductor and source geometry effects on body surface and epicardial potentials. *Circ. Res.*, vol. 46, pp. 283-291, 1980.

(4) B.J. Messinger-Rapport and Y. Rudy, Regularization of the inverse problem: a model study. *Math. Biosci.*, vol. 89, pp. 79-118, 1988.

(5) R. Gulrajani and G.E. Mailloux, A simulation study of the effects of torso inhomogeneities on electrocardiographic potentials, using realistic heart and torso model. *Circ. Res.*, vol. 52 pp. 45-56, 1983.

(6) P. Colli Franzone, L. Guerri, B. Taccardi, and C. Viganotti, Finite element approximation of regularized solution of the inverse potential problem of electrocardiography and applications to experimental data. *Calcolo*, 22, fasc. I, pp. 91-186, 1985.

(7) Y. Rudy and B.J. Messinger-Rapport, The inverse problem in electrocardiography: solutions in terms of potentials. *CRC Crit. Rev. Biomed. Eng.*, vol 16(3), 1988.

(8) C.R. Johnson, The generalized inverse problem in electrocardiography: Theoretical, computational, and experimental results. Ph.D. Dissertation, Univ. of Utah, 1990.

(9) C.L. Rogers and T.C. Pilkington, Free-moment current dipoles in inverse electrocardiography. *IEEE Trans. Biomed. Eng.*, BME-15, pp. 312-323, 1968.

(10) M.S. Lynn, A.C. Barnard, J.H. Holt, and L.T. Sheffield., A proposed method for the inverse problem in electrocardiography. *Biophys. J.*, vol 7, pp.925-945, 1967.

(11) R.C. Barr and M.S. Spach, Inverse solutions directly in terms of potentials. In *The Theoretical Basis of Electrocardiography*, C.V. Nelson and D.B. Geselowitz, Eds., Clarendon Press, Oxford, pp. 294-304, 1976.

(12) R.C. Barr, M. Ramsey, and M.S. Spach, Relating epicardial to body surface potentials distributions by means of transfer coefficients based on geometrical measurements. *IEEE Trans. Biomed. Eng.* BME-24:1-11, 1977.

(13) Y. Yamashita, Theorectical studies on the inverse problem in electrocardiography and uniqueness of the solution. *IEEE Trans. Biomed. Eng.*, BME-29, pp. 719-725, 1982.

(14) C.R. Johnson and A.E. Pollard, Electrical activation of the heart: computational studies of the forward and inverse problems in electrocardiography. In *Computer Assisted Analysis and Modeling*, MIT Press, Boston, pp. 583-628, 1990.

(15) C.R. Johnson, The generalized inverse problem in electrocardiography. In *Proc. of the 12th Annual International Conference of the IEEE Engineering in Medicine and Biology Society*, pp. 593-4, 1990.

(16) C.R. Johnson, The generalized inverse problem. *Journal of Electrocardiology* (to appear July 1991).

(17) B.M. Horacek, Digital model for studies in magnetocardiography. *IEEE Trans. Mag.*, MAG-9:440-444, 1973.

(18) R.S. MacLeod, M. J. Gardner, R.G. MacDonald, M. A. Henderson, R.M. Miller and B.M. Horacek, Application of an inverse solution to body surface potential mapping during PTCA. In *IEEE Engineering in Medicine and Biology Society 12th Annual International Conference* , pages 633-534. IEEE Press, 1990.

(19) R.S. MacLeod, M.J. Gardner and B.M. Horacek, Hochauflösende EKG-Mapping-Verfahren für Untersuchungen während Koronardilitation. *Biomedizinische Technik* 15. Jahrestagung der Österreichischen Gesellschaft für Biomedizinische Technik, Innsbruck, Austria, 1990.

(20) R.S. MacLeod, Percutaneous Transluminal Coronary Angioplasty as a Model of Cardiac Ischemia: Clinical and Modelling Studies. Ph.D. Thesis, Dalhousie University, 1990.

(21) A. S. Vahid and P Savard, A volume conductor model of the human thorax for field calculations. In *Proc. of the 12th Annual International Conference of the IEEE Engineering in Medicine and Biology Society*, pp. 615-6, 1990.

(22) H.S. Oster and Y. Rudy, The Use of Tempoiral Information in the regularization of the inverse problem in electrocardiography. In *Proc. of the 12th Annual International Conference of the IEEE Engineering in Medicine and Biology Society*, pp. 599-600, 1990.

(23) A.N. Tikhonov, and V.Y. Arsenin, *Solutions of Ill-Posed Problems*. John Wiley & Sons, New York, 1977.

(24) J.P. Schadé, *Introduction to functional human anatomy*. W. B. Saunders, Londen, 1974.

(25) K.R. Foster and H P. Schwan, Dielectric properties of tissue and biological materials: a critical review. *CRC Critical Reviews in Biomedical Engineering*, pp. 25-95, 1989.

(26) M.J. Burgess, R.L. Lux and P.R. Ershler, Estimation of depth of onset of activation from cardiac surface electrograms. *Circulation* 80:42, 1989.

(27) B. Taccardi, L.S. Green, P.R. Ershler and R.L. Lux, Epicardial potential mapping: effects of conducting media. *Circulation* 80:134, 1989.

(28) B. Taccardi, R.L. Lux, P.R. Ershler, S. Watabe and E. Macchi: Normal and abnormal intramural spread of excitation and associated potential distributions. *XVII International Congress on Electrocardiology*, pp. 12, 1990.

(29) R.L. Lux, P.R. Ershler and B. Taccardi, 3-dimensional displays of isochrone and isopotential surfaces. In *Proc. of the 12th Annual International Conference of the IEEE Engineering in Medicine and Biology Society*, pp. 108-109, 1988.

(30) R.L. Lux, P.R. Ershler, K.P. Anderson and J.W. Mason, Rapid localization of accessory pathways in WPW syndrome using unipolar potential mapping. In *Proc.of the 12th Annual International Conference of the IEEE Engineering in Medicine and Biology Society*, pp. 195-196, 1989.

(31) T.F. Oostendorp, A. van Oosterom and G. Huiskamp, Interpolation on a triangulated 3D surface. *J Comp. Physics,* 80:331-343, 1989.

(32) R.L. Lux, C.R. Smith, R.F. Wyatt, and J.A. Abildskov, Limited lead selection for estimation of body surface potential maps in electrocardiography. *IEEE Trans. Biomed. Eng.,* BME-25: 270-276, 1978.

(33) R.L. Lux, M.J. Burgess, R.F. Wyatt, A.K. Evans, G.M. Vincent, and J.A. Abildskov, Clinically practical lead systems for improved electrocardiography: comparison with precordial grids and conventional lead systems. *Circulation,* 59: 356-363, 1979.

(34) L.S. Green, R.L. Lux, D. Stilli, C.W. Haws, B. Taccardi, Fine detail in body surface potentials maps: accuracy of maps using a limited lead array and spatial and temporal data representation. *J Electrocardiol.,* 20:21-26

(35) R.L. Lux, Mapping techniques. In *Comprehensive Electrocardiology* , P. W. Macfarlane and T. D. Veitch Lawrie, Eds., Pergamon Press, New York, vol. 2, pp. 1001-1014, 1989.

(36) L.S. Green, R.L. Lux, C.W. Haws, R.R. Williams, C.S. Hunt, and M.J. Burgess, Effects of age, sex, and body habitus on QRS and ST-T potential maps of 1100 normal subjects. *Circulation,* 71: 244-253, 1985.

(37) T.J. Montague, F.X. Witkowski, R.M. Miller, M.A. Henderson, R.G. MacDonald, R.S. MacLeod, M.J. Gardner and B.M. Horacek, Persistent changes in the body surface electrocardiogram following successful coronary angioplasty. *J Electrocardiol.* (In Press).

(38) R.S. MacLeod, B.K. Hoyt, J.D. Sherwood, P.J. MacInnis, R.V. Potter and B.M. Horacek, A body surface mapping unit for recording during coronary angioplasty. In *IEEE Engineering in Medicine and Biology Society 10th Annual International Conference*, pages 97-98. IEEE Press, 1988

(39) P.R. Ershler, R.L. Lux, L.S. Green, G.R. Caputo and D. Parker, Determination of 3-dimensional torso, heart and electrode geometries from magnetic resonance images. In *Proc. of the 10th Annual International Conference of the IEEE Engineering in Medicine and Biology Society*, pp. 121-122, 1988.

(40) A. Bowker, Computing Dirichlet Tesselations. *Computer J,* 24:162-166, 1981.

(41) C.L. Lawson, Software for C1 surface interpolation. *Mathematical Software II,* J.R. Rice, Editor, Academic Press, NY, pp.,161-194, 1977.

(42) R. Plonsey, *Bioelectric Phenomena.* McGraw-Hill, New York, 1969.

(43) D.B. Geselowitz, Multipole representations for an equivalent cardiac generator. *Proc. IRE,* vol. 48, pp. 75-9, 1960.

(44) H. Roozen and A. van Oosterom, Computing the activation sequence at the ventricular heart surface from body surface potentials. *Med. Biol. Eng. Comput.,* vol 25, pp 250-260, 1987.

(45) J. Hadamard, Sur les problemes aux derivees partielies et leur signification physique. Bull. Univ. Princton, pp. 49-52, 1902.

(46) D.S. Dyer, A Dataflow Toolkit for Visualization. *IEEE Comp. Graph. & Appl.*, July: 60-69, 1990.

(47) R. McFee, S. Rush, Qualitative effects of thoracic resistivity variations on the interpretation of electrocardiograms: the low resistance surface layer. *Am. Heart J*, 76:48-61.

(48) V.B. Glasko, *Inverse Problems of Mathematical Physics*. American Institute of Physics, New York, 1988.

(49) S. Watanabe, B. Taccardi, R.L. Lux, P.R. Ershler, Effect of nontransmural necrosis on epicardial potential fields: correlation with fiber direction. *Circulation* 82:2115-2127, 1990.

CHECKLIST *(Front)*

Complete both sides of this form. Check the appropriate boxes and provide the information requested. Make this page the last page of the signed original of the application. *Do not attach copies of this page to the duplicated copies of the application.* Upon receipt and assignment of the application by the PHS, this page will be separated from the application. The page will *not* be duplicated, and it will *not* be a part of the review process. It will be reserved for PHS staff use only.

TYPE OF APPLICATION

[X] NEW application *(This application is being submitted to the PHS for the first time.)*

[ ] REVISION of application number: _____
(This application replaces a prior unfunded version of a new, competing continuation or supplemental application.)

[ ] COMPETING CONTINUATION of grant number: _____
(This application is to extend a funded grant beyond its current project period.)

[ ] SUPPLEMENT to grant number: _____
(This application is for additional funds to supplement a currently funded grant.)

[ ] CHANGE of principal investigator/program director.
Name of former principal investigator/program director: _____

[ ] FOREIGN application. *(This information is required by the U.S. Department of State.)* City and country of
birth and present citizenship of principal investigator/program director: _____

ASSURANCES *(See GENERAL INFORMATION section of instructions.)*

a. Civil Rights Form HHS 441	b. Handicapped Individuals Form HHS 641	c. Sex Discrimination Form 639-A	d. Misconduct in Science
[X] Filed [ ] Not filed	[X] Filed [ ] Not filed	[X] Filed [ ] Not filed	[X] Administrative review process has been established. [X] Reporting requirements of the published scientific misconduct regulations will be followed.

ADDITIONAL ASSURANCES

The following additional certifications described below are made by checking the appropriate boxes and verified by the signature of the OFFICIAL SIGNING FOR APPLICANT ORGANIZATION on the FACE PAGE of the application

e. **Delinquent Federal Debt.** [X] No   [ ] Yes   *(If "Yes," attach explanation.)*

Before a grant award can be made, the applicant organization must certify that it is **not** delinquent on the repayment of any Federal debt. The certification applies to the applicant organization, **not** to the person signing the application as the authorized representative **nor** to the principal investigator/program director.

Examples of Federal debt include delinquent taxes, audit disallowances, guaranteed or direct student loans, FHA loans, business loans, and other miscellaneous administrative debts. For purposes of this certification, the following definitions of "delinquency" apply:

- For **direct loans and fellowships** (whether awarded directly to the applicant by the Federal Government or by an institution using Federal funds), a debt more than 31 days past due on a scheduled payment. (Definition **excludes** "service" payback under a National Research Service Award.)

- For **guaranteed and insured loans**, recipients of a loan guaranteed by the Federal Government that the Federal Government has repurchased from a lender because the borrower breached the loan agreement and is in default.

- For **grants**, organizations in receipt of "Notice of Grants Cost Disallowance" which have not repaid the disallowed amount or which have not resolved the disallowance. (Definition **excludes** cost disallowances in an "appeal" status.)

Where the applicant discloses delinquency on debt to the Federal Government, the PHS shall (1) take such information into account when determining whether the prospective grantee organization is responsible with respect to that grant, and (2) consider not making the grant until payment is made or satisfactory arrangements are made with the agency to whom the debt is owed. Therefore, it may be necessary for the PHS to contact the applicant before a grant can be made to confirm the status of the debt and ascertain the payment arrangements for its liquidation. Applicants that fail to liquidate indebtedness to the Federal Government in a businesslike manner place themselves at risk of not receiving financial assistance from the PHS.

f. **Debarment and Suspension.** [X] No   [ ] Yes *(If "Yes," attach explanation.)*

Before a grant award can be made, the applicant organization must certify, among other things, that neither it nor its principals are presently debarred, suspended, proposed for debarment, declared ineligible, or voluntarily excluded from covered transactions by any Federal department or agency. Subawardees, that is, other corporations, partnerships, or other legal entites (called "lower tier" participants), must make the same certification to the applicant organization concerning their covered transactions. Please refer to the pertinent DHHS implementing regulations, Title 45 Code of Federal Regulations Part 76, for complete certification requirements.

APPENDIX

Figures
Mathematical Theory
Papers (reprints)
Letters from consultants

Figure 1. The CVRTI torso tank

Figure 4. MRI scan showing the heart, lungs, muscle, and fat volumes.

Figure 2. Triangulated geometric model of the CVRTI torso. In white is the epicardial electrode mesh.

Figure 5. Triangularized surface mesh of the same slice as in figure 4, showing, torso, fat, muscle, lungs and epiacrdial surfaces.

Figure 6. Sample slice of the high-resolution thorax model showing the complete tessealtion in tetrahedral volume elements. Colors indicate different conductivity values.

Figure 3. Calculated potential distribution of the torso tank surface from a single dipole source.

Figure 7. Complete torso surface, heart and lungs of the high-resolution thorax model.
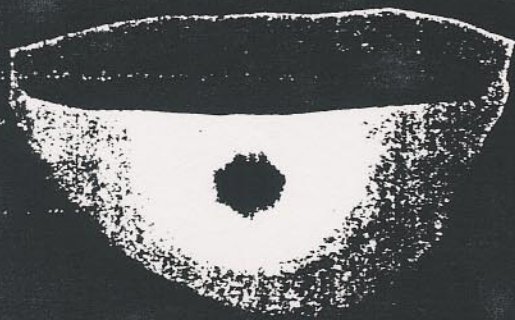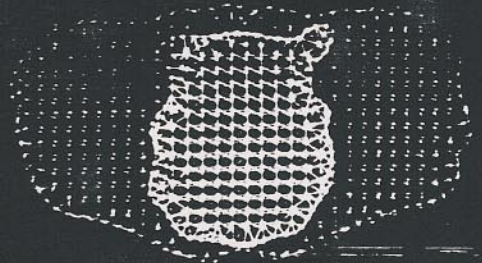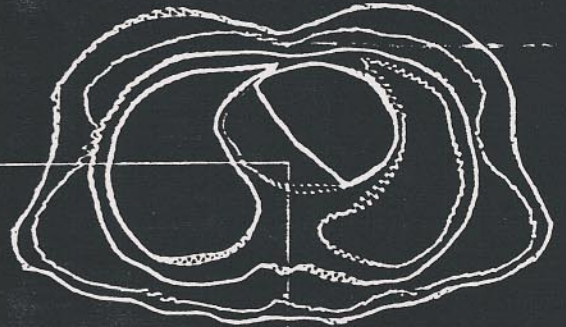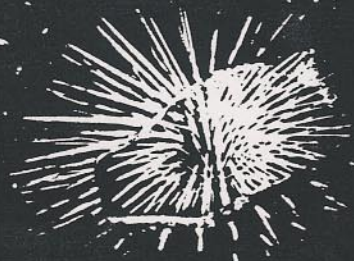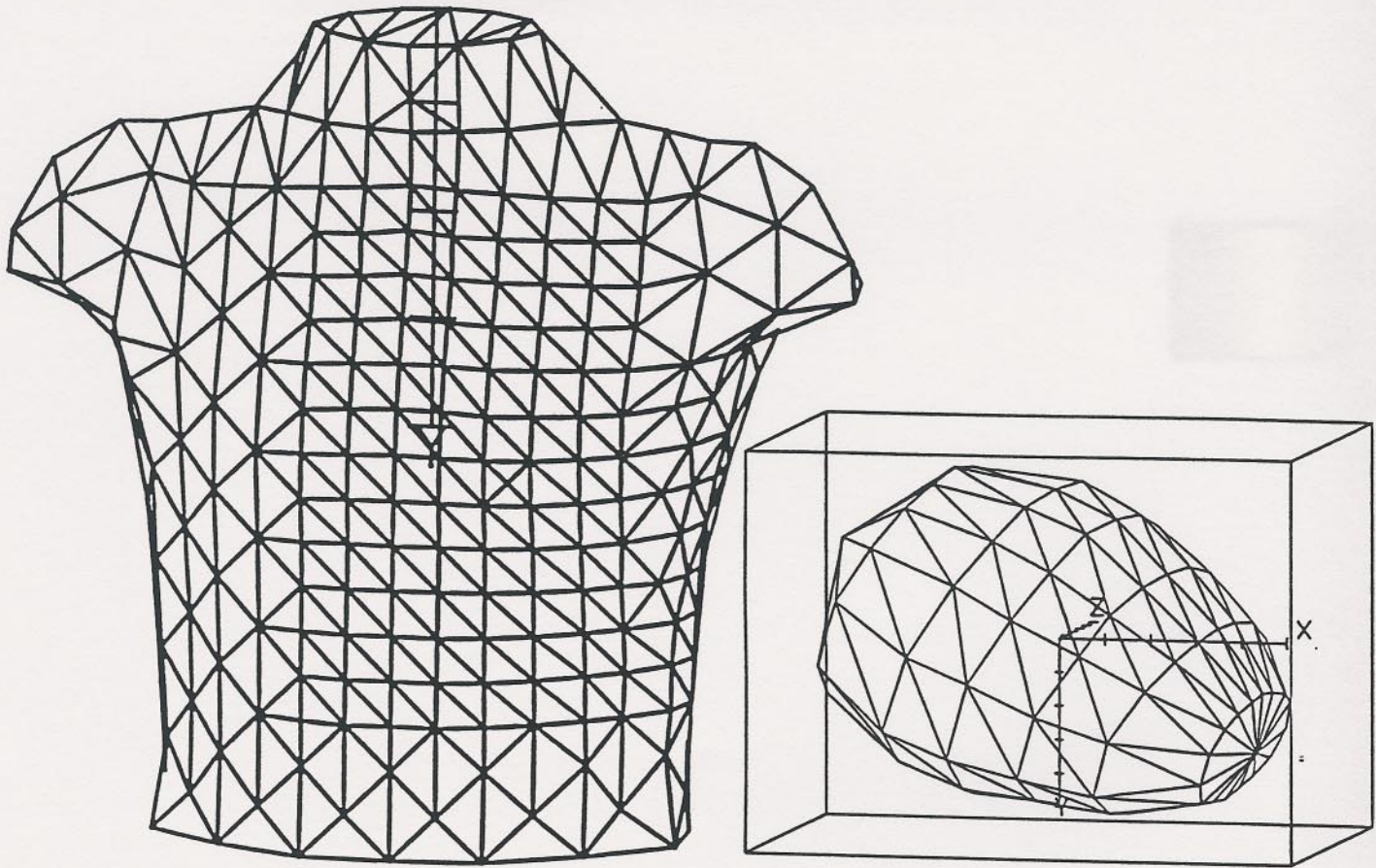
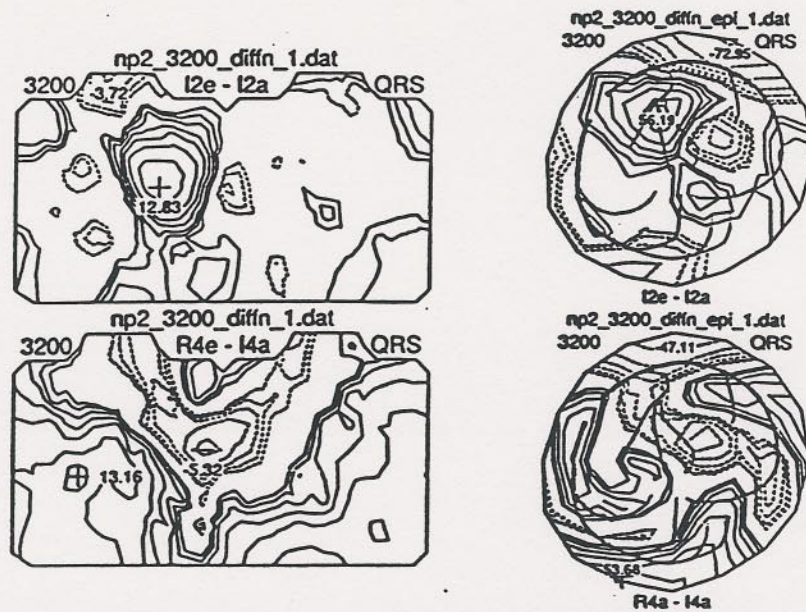Figure 8. Dalhousie torso (left) and epicardium (right).

Figure 9: Body surface (left) and epicardial surface (right) potential difference maps for the same patient during PTCA. Upper maps from an occlusion of the left anterior descending artery; lower maps from occlusion of the right coronary artery.

Mathematical Theory

MATHEMATICAL THEORY

<u>Finite Element Method</u> In this section, the mathematical theory is developed for the forward and inverse problem in electrocardiography via the finite element method. Note: Throughout the section pertaining to the finite element method, index notation will be used. Index notation is the most convenient notation for use with the finite element method as equations can be translated directly into FORTRAN statements. Briefly, a three dimensional vector, $\mathbf{r} = x\mathbf{i} + y\mathbf{j} + z\mathbf{k}$ is now expressed as $\mathbf{r} = x_i\mathbf{i}_i$, where we have used the summation convention that indices which appear exactly twice are automatically summed over. The gradient $\nabla\Phi$ becomes $\mathbf{i}_i\Phi_{,i}$ and the divergenge, $\nabla\cdot\mathbf{E} = E_{i,i}$ where the comma subscript is the index notation for partial differentiation.

The quasi-harmonic equation which needs to be solved for the general inverse problem in electrocardiography is the generalized Poisson's equation for electrical conduction:

$$-(\sigma_{ij}\,\Phi_{,j})_{,i} = I_{SV} \qquad \text{in} \quad \Omega \tag{1}$$

with boundary conditions (2) and (3) as presented in Figure 1:

$$\Phi = \Phi_0 \qquad \text{on} \quad \Sigma \subseteq \Gamma_1 \tag{2}$$

$$(\sigma_{ij}\,\Phi_{,j})\,n_i \; - \; g = 0 \qquad \text{on} \quad \Gamma_1 \tag{3}$$
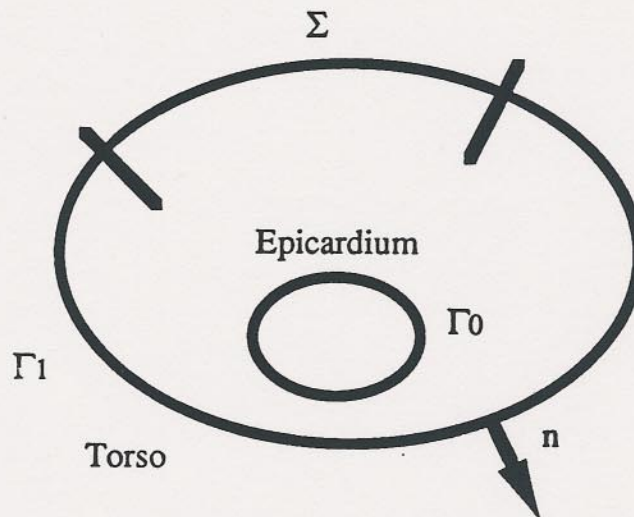

Figure 1. Geometry for the electrocardiographic field equation.

where:

Φ =   Potential field defined in Ω

Φ_0 =   Potentials on the boundary (known *a priori*)

Ω =   Bounded domain

σ_{ij} =   Conductivity tensor

I_{SV}	$=$	Internal current source per unit volume
g	$=$	Externally applied boundary current (if one exists)
n_i	$=$	Unit normal vectors
Γ_0	$=$	Boundary at epicardial surface
Γ_1	$=$	Boundary at torso surface
Σ	$=$	Subset of torso boundary

The Poisson equation is an elliptical partial differential equation which satisfies the Euler-Lagrange condition for the minimization of a functional via the Ritz method if the conductivity tensor is symmetric. A particular formulation of Poisson's equation which allows for complex geometries, anisotropy, and inhomogeneity utilizes the finite element method. A general finite element method involves converting the partial differential equation (1) to a more general integral form. This converts the local pointwise description to a global description. The method is known as the principle of virtual work, yielding what is called the weak formulation. The weak formulation has the advantage over the differential equation formulation in that the weak formulation works only with first derivatives whereas the differential equation uses second derivatives. From an approximation point of view this is a decisive advantage.

Weak Formulation

The field equation for electrocardiography in differential form is:

$$-(\sigma_{ij}\,\Phi_{,j})_{,i} = I_{SV} \qquad \text{in } \Omega \qquad (4)$$

In order to convert this second order partial differential equation into the global integral form, equation (4) is multiplied by an arbitrary continuous (C^0-continuity) function $\overline{\Phi}$. The function $\overline{\Phi}$ can be thought of as a virtual potential field which is a variation of the true potential field Φ. The quantity is then integrated over the entire solution domain:

$$\int_\Omega \left[-(\sigma_{ij}\,\Phi_{,j})_{,i}\right]\overline{\Phi}\,d\Omega = \int_\Omega I_{SV}\,\overline{\Phi}\,d\Omega \qquad (5)$$

Next, the boundary conditions need to be incorporated into the formulation. This can be done by recalling the general integration by parts formula for continuous functions:

$$\int_\Omega \Phi_{,i}\,\Psi\,d\Omega = \int_\Omega \Phi\,(-\Psi_{,i})\,d\Omega + \int_\Gamma (\Phi\,n_i)\,\Psi\,d\Gamma \qquad (6)$$

and applying it to (5) with $\Phi \rightarrow -(\sigma_{ij}\,\Phi_{,j})$ and $\Psi \rightarrow \overline{\Phi}$. This yields a formulation that includes boundary terms:

$$\int_\Omega \sigma_{ij}\,\Phi_{,j}\,\overline{\Phi}_{,i}\,d\Omega - \int_\Gamma \sigma_{ij}\,\Phi_{,j}\,n_i\,\overline{\Phi}\,d\Gamma = \int_\Omega I_{SV}\,\overline{\Phi}\,d\Omega \qquad (7)$$

The second term arises from the fact that different surfaces with different boundary conditions may be considered, depending on the conditions at hand. In general only one boundary term need be

kept for the inverse problem in electrocardiography; however, in the initial derivation all boundary terms will be kept for the most complete general formulation. If more than one surface is considered the boundary term is written as:

$$\int_\Gamma \eta \, d\Gamma = \int_{\Gamma_1} \eta \, d\Gamma + \int_{\Gamma_2} \eta \, d\Gamma + \ldots + \int_{\Gamma_N} \eta \, d\Gamma \quad N = \text{number of surfaces}$$

The boundary term for the Cauchy problem for electrocardiography requires that equation (7) take on the form:

$$\int_\Gamma \sigma_{ij} \, \Phi_{,j} \, n_i \, \overline{\Phi} \, d\Gamma = \int_\Sigma (\sigma_{ij} \, \Phi_{,j}) \, n_i \, \overline{\Phi} \, d\Gamma + \int_{\Gamma_1} \overline{\Phi} \, g \, d\Gamma \qquad (8)$$

Physically, $\overline{\Phi}$ is a virtual potential field. If a portion of the boundary is fixed, the virtual potential field must be zero on this portion, since the virtual potential field is a variation of the true potential field and must not violate the *a priori* constraints. Since Φ is fixed on $\Sigma \subseteq \Gamma_1$, $\overline{\Phi}$ must be zero on $\Sigma \subseteq \Gamma_1$. Therefore the boundary term is given as

$$\int_\Gamma (\sigma_{ij} \, \Phi_{,j}) \, n_i \, \overline{\Phi} \, d\Gamma = \int_\Gamma g \, \overline{\Phi} \, d\Gamma \qquad (9)$$

Substitution of the boundary term into (7) yields:

$$\int_\Omega \sigma_{ij} \, \Phi_{,j} \, \overline{\Phi}_{,i} \, d\Omega = \int_\Omega I_{SV} \, \overline{\Phi} \, d\Omega + \int_\Gamma g \, \overline{\Phi} \, d\Gamma \qquad (10)$$

Equation (10) holds for an arbitrary continuous function $\overline{\Phi}$ such that $\overline{\Phi} = 0$ on $\Sigma \subseteq \Gamma_1$. Equation (10) represents the weak form $\Phi = \Phi_0$ on $\Sigma \subseteq \Gamma_1$ such that equation (10) holds $\forall \, \overline{\Phi} \in \overline{\Phi} = 0$ on $\Sigma \subseteq \Gamma_1$. Thus the second order electrocardiographic field equation subject to appropriate boundary conditions has been converted into a single integral equation which includes the boundary conditions implicitly within the formulation.

In order to ensure the accuracy of the weak formulation derivation, the relationship in equation (10) will also be derived via the minimization technique. This is equivalent to the Ritz formulation from the calculus of variations. Since the conductivity tensor is symmetric, we can define a potential energy functional:

$$f(\Phi) = \frac{1}{2} \int_\Omega \sigma_{ij} \, \Phi_{,j} \, \Phi_{,i} \, d\Omega - \int_\Omega I_{SV} \, \Phi \, d\Omega - \int_\Gamma g \, \Phi \, d\Gamma \qquad (11)$$

The idea is to minimize the potential energy of the system. It should be noted that the minimization procedure only applies to symmetric conductivity tensors and conservative equations which satisfy

the Euler-Lagrange equations. This condition is met by the electrocardiographic field equation. The minimization procedure requires:

$$f(\Phi) = \min \, f(\tilde{\Phi}) \qquad \text{subject to } \tilde{\Phi} = \Phi_0 \text{ on } \Sigma \subseteq \Gamma_1$$

and then $f(\Phi) \leq f(\Phi \pm \theta(\hat{\Phi} - \Phi)) \qquad \forall \, \hat{\Phi} \in \, \hat{\Phi} = \Phi_0 \quad$ on $\Sigma \subseteq \Gamma_1$ and

$$\forall \, \theta \in (0,1)$$

This is equivalent to taking the first variation of $f(\Phi)$ at the solution set Φ. The quantity $f(\Phi) \leq f(\Phi \pm \theta(\hat{\Phi} - \Phi))$ may be derived using equation (11). Upon direct substitution we have:

$$f(\Phi \pm \theta(\hat{\Phi} - \Phi)) = \frac{1}{2} \int_\Omega \sigma_{ij} \, (\Phi \pm \theta(\hat{\Phi} - \Phi))_{,j} \, (\Phi \pm \theta(\hat{\Phi} - \Phi))_{,i} \, d\Omega$$

$$- \int_\Omega I_{VS} \, (\Phi \pm \theta(\hat{\Phi} - \Phi)) \, d\Omega - \int_{\Gamma_1} g \, (\Phi \pm \theta(\hat{\Phi} - \Phi)) \, d\Gamma \qquad (12)$$

Performing the differentiations and expanding yields:

$$f(\Phi \pm \theta(\hat{\Phi} - \Phi)) = \frac{1}{2} \int_\Omega \sigma_{ij} \, \Phi_{,j} \, \Phi_{,i} \, d\Omega \pm \theta \int_\Omega \Phi_{,j} \, (\hat{\Phi} - \Phi)_{,i} \, d\Omega$$

$$\pm \frac{1}{2} \theta^2 \int_\Omega (\hat{\Phi} - \Phi)_{,j} \, (\hat{\Phi} - \Phi)_{,i} \, d\Omega - \int_\Omega I_{VS} \, \Phi \, d\Omega - \pm \int_\Omega \theta \, I_{VS} \, (\hat{\Phi} - \Phi) \, d\Omega$$

$$- \int_{\Gamma_1} g \, \Phi \, d\Gamma - \pm \theta \int_{\Gamma_1} g \, (\hat{\Phi} - \Phi) \, d\Gamma \qquad (13)$$

recalling that the original potential energy functional is given as:

$$f(\Phi) = \frac{1}{2} \int_\Omega \sigma_{ij} \, \Phi_{,j} \, \Phi_{,i} \, d\Omega - \int_\Omega I_{VS} \, \Phi \, d\Omega - \int_\Gamma g \, \Omega \, d\Gamma \qquad (14)$$

The inequality $f(\Phi \pm \theta(\hat{\Phi} - \Phi)) - f(\Phi) \geq 0$ is given as:

$$\pm \theta \int_\Omega \Phi_{,j} \, (\hat{\Phi} - \Phi)_{,i} \, d\Omega \pm \frac{1}{2} \theta^2 \int_\Omega (\hat{\Phi} - \Phi)_{,j} \, (\hat{\Phi} - \Phi)_{,i} \, d\Omega$$

$$- \pm \theta \int_{\Omega} I_{VS} (\widehat{\Phi} - \Phi) \, d\Omega - \pm \theta \int_{\Gamma_1} g (\widehat{\Phi} - \Phi) \, d\Gamma \geq 0 \qquad (15)$$

Dividing by θ and passing to the limit $\theta \to 0$ yields:

$$\pm \int_{\Omega} \Phi_{,j} (\widehat{\Phi} - \Phi)_{,i} \, d\Omega \geq \pm \int_{\Omega} I_{VS} (\widehat{\Phi} - \Phi) \, d\Omega \pm \int_{\Gamma_1} g (\widehat{\Phi} - \Phi) \, d\Gamma \qquad (16)$$

Since $\widehat{\Phi}$ is arbitrary, $\widehat{\Phi} = -\widehat{\Phi}$ is also acceptable. Using the upper and lower signs in equation (16), the inequality takes the form:

$$\int_{\Omega} \Phi_{,j} (\widehat{\Phi} - \Phi)_{,i} \, d\Omega = \int_{\Omega} I_{SV} (\widehat{\Phi} - \Phi) \, d\Omega + \int_{\Gamma_1} g (\widehat{\Phi} - \Phi) \, d\Gamma \qquad (17)$$

Since $\widehat{\Phi}$ is arbitrary, $\overline{\Phi} = \widehat{\Phi} - \Phi$ is also arbitrary; however, $\overline{\Phi} = 0$ on $\Sigma \subseteq \Gamma_1$. This means that $\widehat{\Phi} - \Phi = 0$ on $\Sigma \subseteq \Gamma_1$. Substitution of $\overline{\Phi} = \widehat{\Phi} - \Phi$ into equation (36) yields:

$$\int_{\Omega} \Phi_{,j} \overline{\Phi}_{,i} \, d\Omega = \int_{\Omega} I_{SV} \overline{\Phi} \, d\Omega + \int_{\Gamma_1} g \overline{\Phi} \, d\Gamma \qquad (18)$$

for $\Phi = \Phi_0$ on $\Sigma \subseteq \Gamma_1$, $\overline{\Phi} = 0$ on $\Sigma \subseteq \Gamma_1 \qquad \forall \overline{\Phi} \in \overline{\Phi} = 0$ on $\Sigma \subseteq \Gamma_1$

Equation (18) is exactly the same as equation (10); therefore, we have the equivalence of forms, and either formulation may be used to convert the differential equation into a global integral form. It should be noted that a third procedure, the Galerkin method, also produces the same formulation.

Finite Element Discretization

Once the equation is in the global integral form, the finite element approximation method is applied to turn the continuous formulation into a discrete formulation.

The first step is to discretize the entire solution domain, where all calculations are to take place.

$$\Omega = \bigcup_{e=1}^{E} \Omega_e \qquad (19)$$

Next, one must define the approximation function, the interpolation function, which is used to solve the discrete form of the global integral equation. This means that the solution variable, here the potential distribution, is the interpolating function. In general, complete polynomials are used as interpolation functions in the solution domain Ω. In three dimensions a complete n-th order polynomial may be written as:

$$P_n\,(x,y,z) \;=\; \sum_{l=1}^{T_n^{(3)}} \alpha_l\, x^i\, y^j\, z^k \qquad\qquad i+j+k \le n \qquad\qquad (20)$$

where $T_n^{(3)} = \dfrac{(n+1)(n+2)(n+3)}{6}$ is the number of terms in the polynomial.

Here for n=1, the interpolation polynomial is the first order linear tetrahedron, and for n=2 it is the second order tetrahedron. Whether a smaller number of higher order elements or a larger number of first order elements should be used to characterize the solution domain is still to be determined. The present study utilizes first order elements. The discretization of Ω, Φ, and $\overline{\Phi}$ is accomplished using isoparametric elements. Isoparametric elements satisfy the basic convergence requirements for the shape functions, which are:

1) Smoothness - at least C^1 on each element interior Ω^e
2) Continuity across each element boundary Γ^e
3) Completeness

In the first requirement C^1 implies that the interpolation function has a continuous first derivative. The first two conditions ensure that all integrals necessary for the computation of element arrays are well defined. The third requirement says that the element interpolation function is capable of exactly representing an arbitrary linear polynomial when the nodal degrees of freedom are assigned values in accordance with it. In other words, as the finite element discretization of the solution domain becomes finer and finer, the exact solution and its derivatives approach constant values over each element within the solution domain. For isoparametric elements the coordinates and potentials (interpolation functions) are of the same form.

$$x\,(\overline{\xi}) \;=\; \sum_{a=1}^{n_{en}} N_a\,(\overline{\xi})\,\overline{x}_a^e \qquad\qquad (21)$$

and

$$\Phi^h\,(\overline{\xi}) \;=\; \sum_{a=1}^{n_{en}} N_a\,(\overline{\xi})\,\Phi^h(\overline{x}_a^e) \qquad\qquad (22)$$

where $N_a\,(\overline{\xi})$ are the interpolation functions (shape functions).

The trilinear hexahedron is the fundamental isoparametric element in three dimensions. The hexahedron can be converted into other elements such as triangular prisms and tetrahedrons via the method of degeneration. The choice of which element to use is dependent on the geometry of the solution domain. For regular geometries, the first or second order hexahedron is usually the best element, while for irregular geometries, the first or second order tetrahedron is often the element of choice.

In order to apply the interpolation function, all coordinates must be mapped to what is called the parent domain, which is a fixed unit coordinate system. The coordinate transformation

from the natural coordinates associated with the element parent domain (finite element domain) to the coordinates of a point (x,y, and z location of the nodal points) is via an affine map. Thus the domain Ω_e is the image of the biunit cube in ξ-space under a trilinear transformation as seen in Figure 2.

    The natural coordinates (parent domain) are:

$$\bar{\xi} = \left\{ \begin{array}{c} \xi \\ \eta \\ \zeta \end{array} \right\} \quad \text{in the trilinear hexahedron} \tag{23}$$

and

$$\bar{x} = (x, y, z)$$

$$\bar{\xi} = (\xi, \eta, \zeta)$$
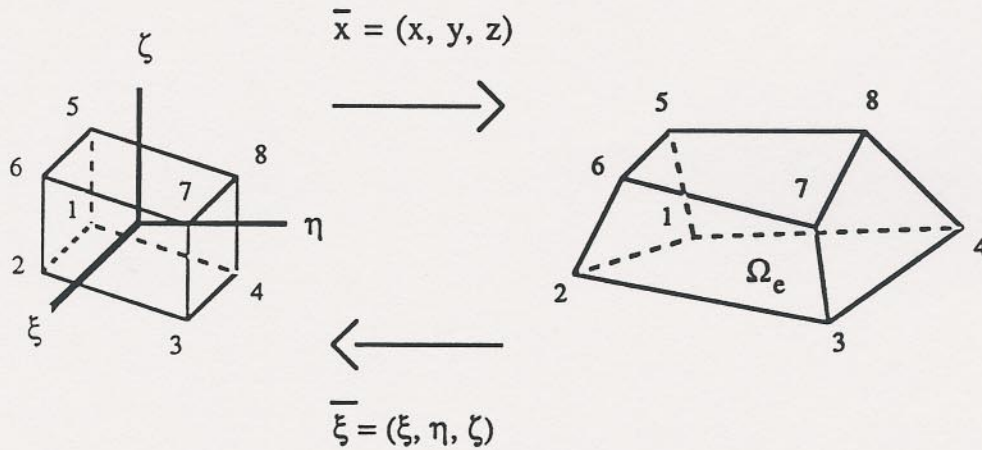
Figure 2. Coordinate map

$$\bar{x} = \left\{ \begin{array}{c} x \\ y \\ z \end{array} \right\} \quad \text{in } \Omega^e \tag{24}$$

The mappings are of the form:

$$x\,(\xi,\eta,\zeta) = \sum_{a=1}^{8} N_a(\xi,\eta,\zeta)\, x_a^e \tag{25}$$

$$y\,(\xi,\eta,\zeta) = \sum_{a=1}^{8} N_a(\xi,\eta,\zeta)\, y_a^e \tag{26}$$

$$z(\xi,\eta,\zeta) = \sum_{a=1}^{8} N_a(\xi,\eta,\zeta) \, z_a^e \tag{27}$$

or in general:

$$\bar{x}(\bar{\xi}) = \sum_{a=1}^{8} N_a(\bar{\xi}) \, \bar{x}_a^e \tag{28}$$

and

$$\Phi^h(\bar{\xi}) = \sum_{a=1}^{8} N_a(\bar{\xi}) \, \Phi^h(x_a^e) \tag{29}$$

where

$$x(\bar{\xi}) = \alpha_0 + \alpha_1\,\xi + \alpha_2\,\eta + \alpha_3\,\zeta + \alpha_4\,\xi\eta + \alpha_5\,\eta\zeta + \alpha_6\,\xi\zeta + \alpha_7\,\xi\eta\zeta \tag{30}$$

$$y(\bar{\xi}) = \beta_0 + \beta_1\,\xi + \beta_2\,\eta + \beta_3\,\zeta + \beta_4\,\xi\eta + \beta_5\,\eta\zeta + \beta_6\,\xi\zeta + \beta_7\,\xi\eta\zeta \tag{31}$$

$$z(\bar{\xi}) = \gamma_0 + \gamma_1\,\xi + \gamma_2\,\eta + \gamma_3\,\zeta + \gamma_4\,\xi\eta + \gamma_5\,\eta\zeta + \gamma_6\,\xi\zeta + \gamma_7\,\xi\eta\zeta \tag{32}$$

The coefficients α, β, and γ are determined by the condition:

$$x(\bar{\xi}_a) = x_a^e \qquad a = 1, 2, \cdots, 8 \tag{33}$$

Solving for α, β, and γ and substituting them into equations (30), (31), and (32) yields:

$$x(\bar{\xi}) = \sum_{a=1}^{8} N_a(\bar{\xi}) \, x_a^e \tag{34}$$

$$\Phi^h(\bar{\xi}) = \sum_{a=1}^{8} N_a(\bar{\xi}) \, \Phi^h(x_a^e) \tag{35}$$

with
$$N_a(\xi,\eta,\zeta) = \frac{1}{8}(1 + \xi_a\,\xi)(1 + \eta_a\,\eta)(1 + \zeta_a\,\zeta) \tag{36}$$

The interpolation function (shape function) $N_a(\xi,\eta,\zeta)$ can take on the representations of an eight node hexahedral element, a six node triangular prism, or a four node tetrahedron. The shape function initially takes the form of a hexahedral element and can be reduced to the other elements via the method of degeneration.

Stiffness Matrix and Load Vector Formulation

The interpolation functions must be calculated for each element within the solution domain; then the element formulations must be incorporated into the global formulation. Starting with the weak formulation, equation (10)

$$\int_\Omega \sigma_{ij}\, \Phi_{,j}\, \overline{\Phi}_{,i}\, d\Omega \;=\; \int_\Omega I_{VS}\, \overline{\Phi}\, d\Omega \;+\; \int_{\Gamma_1} g\, \overline{\Phi}\, d\Gamma \tag{37}$$

the entire solution domain is discretized using isoparametric elements:

$$\sum_{e=1}^{E} \int_{\Omega_e} \sigma_{ij}\, \Phi_{,j}\, \overline{\Phi}_{,i}\, d\Omega \;=\; \sum_{e=1}^{E} \int_{\Omega_e} I_{VS}\, \overline{\Phi}\, d\Omega \;+\; \sum_{e=1}^{E_1} \int_{\Gamma_e^1} g\, \overline{\Phi}\, d\Gamma \tag{38}$$

Application of the interpolation function yields the discrete potential fields:

$$\Phi(\xi,\eta,\zeta) \rightarrow \Phi^h(\xi,\eta,\zeta) \;=\; \sum N_a(\xi,\eta,\zeta)\, \Phi^h(x_a^e) \;=\; N_a\, \Phi_a \tag{39}$$

$$\overline{\Phi}(\xi,\eta,\zeta) \rightarrow \overline{\Phi}^h(\xi,\eta,\zeta) \;=\; \sum N_b(\xi,\eta,\zeta)\, \overline{\Phi}^h(x_b^e) \;=\; N_b\, \overline{\Phi}_b \tag{40}$$

The first term in (38) becomes:

$$\sum_{e=1}^{E} \int_{\Omega_e} \sigma_{ij}\, \Phi_{,j}\, \overline{\Phi}_{,i}\, d\Omega \;=\; \sum_{e=1}^{E} \int_{\Omega_e} \sigma_{ij}\, \Phi_a\, N_{a,j}\, \overline{\Phi}_b\, N_{b,i}\, d\Omega$$

$$=\; \sum_{e=1}^{E} \overline{\Phi}_b \left(\int_{\Omega_e} \sigma_{ij}\, N_{a,j}\, N_{b,i}\, d\Omega \right) \Phi_a \;=\; \sum_{e=1}^{E} \overline{\Phi}_b\, K_{ba}^e\, \Phi_a \tag{41}$$

where $K_{ba}^e = \left(\int_{\Omega_e} \sigma_{ij}\, N_{b,i}\, N_{a,j}\, d\Omega \right)$ is the element stiffness matrix.

The summation of each of the individual element matrices represents the global stiffness matrix. The global stiffness matrix is the basis of the transfer matrix relating torso and epicardial potentials. It has the properties that it is symmetric and usually very sparse such that sparse linear system algorithms such as the Sherman-Morrison formula or the conjugate gradient method may be utilized.

The second term in (38) becomes:

$$\sum_{e=1}^{E} \int_{\Omega_e} I_{VS}\, N_b\, \overline{\Phi}_b\, d\Omega \;=\; \sum_{e=1}^{E} \overline{\Phi}_b\, I_{VSb}^e \tag{42}$$

where $I_{VSb}^e = \displaystyle\int_{\Omega_e} I_{VS} \, N_b \, d\Omega$ is the generalized element load vector.

This represents the current for each element (if one exists), the summation of which represents all the current sources. The current source may be modeled in a variety of ways from a simple point source to extraordinarily complex models. The modeling of the current source represents ongoing research which constitutes an entire field in itself, and is thus beyond the scope of this treatment. Since for this study the actual current sources of the heart are not the prime focus, the current source was modeled as either a point source, or an n-th order polynomial.

Lastly, for the boundary term in (38)

$$\int_{\Gamma_1} g \, \overline{\Phi} \, d\Gamma = \sum_{e=1}^{E_1} \int_{\Gamma_1^e} g \, \overline{\Phi} \, d\Gamma = \sum_{e=1}^{E_1} \overline{\Phi}_b \, g_b^e \tag{43}$$

where $g_b^e = \displaystyle\int_{\Gamma_1^e} g \, N_b \, d\Gamma$ and E_1 is the number of elements on Γ_1.

This particular boundary term represents the nonzero Neumann boundary condition. For most applications in electrocardiography this term is zero. Now that all the element matrices and vectors have been calculated and accumulated into the global matrices and vectors, the weak form of the boundary value problem

$$\int_{\Omega} \sigma_{ij} \, \Phi_{,j} \, \overline{\Phi}_{,i} \, d\Omega = \int_{\Omega} I_{VS} \, \overline{\Phi} \, d\Omega + \int_{\Gamma_1} g \, \overline{\Phi} \, d\Gamma \tag{44}$$

can be represented by the finite element approximation of:

$$\sum_{e=1}^{E} \overline{\Phi}_b \, K_{ba}^e \, \Phi_a = \sum_{e=1}^{E} \overline{\Phi}_b \, I_{VSb}^e + \sum_{e=1}^{E_1} \overline{\Phi}_b \, g_b^e \tag{45}$$

Once the boundary conditions are applied (for most applications in electrocardiography these would be that the torso or epicardial potentials are specified and the electric field normal to the torso is zero), the finite element approximation reduces to a system of linear algebraic equations.

$$\sum_{e=1}^{E} K_{ba}^e \, \Phi_a = \sum_{e=1}^{E} I_{VSb}^e + \sum_{e=1}^{E_1} g_b^e \tag{46}$$

Equation (65) is the finite element approximation for the anisotropic, inhomogeneous electrocardiographic field equation.

There exist several different problems of interest that can be solved from equation (46):

1)   The right hand side of equation (65) is zero ($I = g = 0$). This then reduces to the generalized Laplaces equation. This equation may be then solved for:

i)   Anisotropic, inhomogeneous forward and inverse problems relating torso potentials to epicardial potentials.
ii)   Homogeneous and/or isotropic forward and inverse problems.

II)   The externally applied boundary current is zero (g=0), and the source current is nonzero. This is the generalized Poisson equation. This may be solved for:
i)   Anisotropic, inhomogeneous forward and inverse problems where the fundamental current sources of the heart are modeled. This would lead to a solution relating myocardial currents to epicardial, volume, and torso potentials.
ii)   Isotropic, homogeneous forward and inverse problems relating current sources to volume and surface potentials.

III)   The source current term is zero ($I_{SV}=0$), and the boundary current is nonzero. This may solve:
i)   Problems which involve injecting current into the body to see how the current effects torso and volume potentials. This would generally be done under the conditions of category one, such that the potentials would be from epicardial to torso surface while the current would be injected as one or more point sources on the torso surface or within the volume conductor.

IV)   All terms exist. This would be the special case for a nonzero externally applied boundary current and a nonzero source current. The full formulation could be used to solve:
i)   Anisotropic, inhomogeneous forward and inverse problems where the fundamental current sources of the heart are modeled while simultaneously injecting current at one or more locations on the torso surface.
ii)   Isotropic, homogeneous forward and inverse problems relating current sources to volume and surface potentials while simultaneously injecting current at one or more locations on the torso surface.

We shall focus our attention to the first category, the solution of the generalized anisotropic, inhomogeneous inverse problem in terms of potentials.

From equation (65) with $I_{SV}=g=0$, the set of equations to be solved is:

$$\sum_{e=1}^{E} K_{ba}^{e}\, \Phi_a = 0 \tag{47}$$

with $\Phi = \Phi_0$ on $\Sigma \subseteq \Gamma_1$ and $(\sigma_{ij}\, \Phi_{,j})\, n_i = 0$, which are the Dirichlet and Neumann boundary conditions respectively. Here the global stiffness matrix contains all the geometrical information of the problem, as well as all of the conductivity information. The latter is in the form of a three by three conductivity tensor for each element in the solution domain. In theory each element could be given a different anisotropic inhomogeneity, the only constraint being the lack of accurate physiological input data. The global stiffness matrix can be partitioned into submatrices that contain local geometrical and conductivity information:

$$\begin{pmatrix} K_{TT} & K_{TV} & K_{TE} \\ K_{VT} & K_{VV} & K_{VE} \\ K_{ET} & K_{EV} & K_{EE} \end{pmatrix} \begin{pmatrix} \Phi_T \\ \Phi_V \\ \Phi_E \end{pmatrix} = \begin{pmatrix} 0 \\ 0 \\ 0 \end{pmatrix} \text{ with } \Phi = \Phi_0 \text{ on } \Sigma \subseteq \Gamma_1 \tag{48}$$

where the subscripts T,V, and E stand for torso, volume, and epicardial respectively. Thus, for example, the subscript VE stands for the part of the stiffness matrix that connects nodes from the volume conductor and the epicardial surface, while TT would be all those nodes that lie on the torso surface, etc. The general inverse problem requires that the potentials on the epicardial surface be found in terms of the measured torso potentials. Thus, one must eliminate all nodes contained within the volume. This can done by solving equation (48) for the Φ_V potential values in terms of Φ_T and Φ_E:

$$\Phi_V = - K_{VV}^{-1} \left[K_{VE}\, \Phi_E + K_{VT}\, \Phi_T \right] \tag{49}$$

The volume matrix K_{VV} is in general well-conditioned (the condition number is usually much less than 100 for small systems and less than 200 for large systems); thus, its inverse is well-behaved. Placing the formula for the volume potentials into equation (48) yields a matrix relationship between the epicardial and torso potentials:

$$\Phi_E = (K_{TV}\, K_{VV}^{-1}\, K_{VE} - K_{TE})^{-1}\, (K_{TT} - K_{TV}\, K_{VV}^{-1}\, K_{VT})\, \Phi_T \tag{50}$$

$$\text{or}\ \ \Phi_E = A_E^{-1}\, A_T\, \Phi_T = (A_{TE})^{-1}\, \Phi_T \tag{51}$$

where the matrix A_{TE} in equation (51) is the transfer matrix of geometry and conductivity coefficients relating torso potentials to epicardial potentials. It should be noted that in contrast to other approaches the partitioning of the global stiffness matrix in this manner allows us to invert only a part of the transfer matrix of coefficients, thus minimizing the effects of performing an inverse on an ill-conditioned matrix. This means that only half of the transfer matrix needs to undergo a regularization procedure.

Regularization

Once the problem has been discretized and the coefficients of the transfer matrix are found by the finite element method, the transfer function must be inverted to obtain the solution vector of epicardial potentials. Due to the inhomogeneities within the volume conductor, the matrix A_{TE}, relating the epicardial and body-surface potentials is ill-conditioned. Inversion of the transfer matrix leads to a problem that is ill-posed. By ill-posed we mean that the solution Φ_E no longer depends continuously on the data, Φ_T, such that small errors in the experimental data (mainly due to geometrical errors and instrument noise) yield large unbounded errors in the solution. Thus, a method that will restore the continuous dependence of the solution on the data is needed.

Regularization techniques are methods that attempt to restore the continuity of an inverse solution. The regularization methods utilized in this study are the class of Tikhonov regularizers [35]. The system of equations to be solved are, from equation (51),

$$\Phi_E = A_{TE}^{-1}\, \Phi_T \tag{52}$$

where $\Phi_T \in \phi_T$, $\Phi_E \in \phi_E$ and $D \subset \phi_E$. ϕ_E and ϕ_T are chosen as Hilbert spaces and D is the set of *a priori* constraints of the problem. A_{TE} is assumed to be a linear one-to-one operator from ϕ_E to ϕ_T.

Since the torso potentials are taken experimentally, the data will vary from the exact value by a value proportional to the noise level in the data:

$$\|\tilde{\Phi}_T - \Phi_T\| \le \delta \tag{53}$$

the norm being

$$\|\Phi\| = \left\{ \sum_{i=1}^{n} \Phi_i^2 \right\}^{\frac{1}{2}} \tag{54}$$

where Φ_T is the exact torso potential value and $\tilde{\Phi}_T$ is the measured torso potential value. Due to discretization errors, $\tilde{A}_{TE}$ will be the approximation of the true transformation matrix A_{TE} such that:

$$\|\tilde{A}_{TE} - A_{TE}\| \le h \tag{55}$$

The approximate data are represented by $(\tilde{A}_{TE}, \tilde{\Phi}_T, \varepsilon)$ where $\varepsilon = \{\delta, h\}$ is the error vector. One wishes to find, using approximate data, a vector $\Phi_{E\varepsilon} \in D$ such that $\Phi_{E\varepsilon} \to \Phi_E$ as $\varepsilon \to 0$.

The problem reduces to finding the vector $\Phi_{E\varepsilon}^{\alpha}$ which minimizes the functional:

$$M^{\alpha}\left[\Phi_E, \tilde{\Phi}_T, \tilde{A}_{TE}\right] = \|\tilde{A}_{TE} \Phi_E - \tilde{\Phi}_T\|_{\phi_T}^2 + \alpha \|\Phi_E - \Phi'_E\|_{\phi_E}^2 \qquad \alpha > 0 \tag{56}$$

where α is the regularization parameter and Φ'_E are *a priori* constraints placed on the epicardial potentials. It can be shown [Tikhonov, 1977] that the Tikhonov regularizing functional $M^{\alpha}\left[\Phi_E, \tilde{\Phi}_T, \tilde{A}_{TE}\right]$ is convex for any $\alpha > 0$ such that it will have a lower bound only at a point $\Phi_{E\varepsilon}^{\alpha}$. A more generalized form of the Tikhonov functional can be expressed as:

$$M^{\alpha}\left[\Phi_E, \tilde{\Phi}_T, \tilde{A}_{TE}\right] = \|\tilde{A}_{TE} \Phi_E - \tilde{\Phi}_T\|_{\phi_T}^2 + \alpha \|C(\Phi_E - \Phi'_E)\|_{\phi_E}^2 \qquad \alpha > 0 \tag{57}$$

Here C is a constraint matrix that can take on one of the following forms:

$C = I$ where I is the identity matrix. In this case equation (57) reduces to (56). In general this formulation constrains upper and lower bounds on the magnitudes of epicardial potentials, thus preventing unbounded oscillations.

$C = \Phi_{,i} i_i$ which is the surface gradient. This constraint prevents large nonphysiological potential gradients.

$C = \Phi_{,ii}$ which is the surface Laplacian. This constraint restricts curvature of the solution vector.

Minimization of the generalized functional in (57) yields:

$$2A_{TE}^T \widetilde{A}_{TE}\Phi_E - 2\widetilde{A}_{TE}^T \widetilde{\Phi}_T + 2\alpha C^T C(\Phi_E - \Phi'_E) = 0 \tag{58}$$

where the superscript T stands for the matrix transpose (not to be confused with the subscript T which signifies torso). Solving the previous equation for the epicardial potentials yields:

$$\Phi_{E\varepsilon}^\alpha = (\widetilde{A}_{TE}^T \widetilde{A}_{TE} + \alpha C^T C)^{-1}(\widetilde{A}_{TE}^T \widetilde{\Phi}_T + \alpha C^T C \Phi'_E) \tag{59}$$

where $\Phi_{E\varepsilon}^\alpha$ is the estimate of the epicardial potentials dependent on the regularization parameter α and the error vector ε.

While there are several ways to determine the regularization parameter α, one obviously wishes to find the best α, one that balances smoothness and accuracy. One method which has proven to be order-optimal for the Tikhonov regularization scheme is the generalized discrepancy principle [Tikhonov, 1977]. Briefly, the discrepancy principle defines a measure of incompatibility

$$\mu_\varepsilon \equiv \inf_{\phi_E \in D} \|\widetilde{A}_{TE}\Phi_E - \widetilde{\Phi}_T\|_{\phi_T} \tag{60}$$

The general discrepancy $\rho_\varepsilon(\alpha)$ is defined as:

$$\rho_\varepsilon(\alpha) \equiv \beta_\varepsilon(\alpha) - [\delta + h\sqrt{\gamma_\varepsilon(\alpha)}]^2 - \mu_\varepsilon^2 \tag{61}$$

where $\beta_\varepsilon(\alpha) \equiv \|\widetilde{A}_{TE}\Phi_{E\varepsilon}^\alpha - \widetilde{\Phi}_T\|^2$, $\gamma_\varepsilon(\alpha) \equiv \|\Phi_{E\varepsilon}^\alpha\|^2$ and $\Phi_{E\varepsilon}^\alpha$ is the extremal of the Tikhonov's functional $M^\alpha[\Phi_E]$ at a fixed $\alpha > 0$. In order to ensure that $\Phi_{E\varepsilon} = 0$ is not taken as the approximate solution one allows for the natural condition:

$$\|\widetilde{\Phi}_T\|^2 > \delta^2 + \mu_\varepsilon^2 \tag{62}$$

The general discrepancy, $\rho_\varepsilon(\alpha)$, takes on the following limiting values:

$$\lim_{\alpha \to \infty} \rho_\varepsilon(\alpha) = \|\widetilde{\Phi}_T\|^2 - \delta^2 - \mu_\varepsilon^2 \tag{63}$$

$$\lim_{\alpha \to 0+0} \rho_\varepsilon(\alpha) = -\delta^2 \tag{64}$$

such that the equation $\rho_\varepsilon(\alpha) = 0$ has a root, $\alpha^*(\varepsilon)$, at a fixed $\alpha > 0$, the element $\Phi_{E\varepsilon}^{\alpha^*(\varepsilon)}$ being uniquely defined. Thus one must find the root of equation (61) in order to find the optimal regularization parameter. Finding the root may be accomplished, for example, by a modified Newton-Raphson method to iterate to a minimal error value. The discrepancy technique allows for the *a priori* estimate of the regularization parameter based upon discretization errors due to the

complex geometries as well as errors incurred from instrument and measurement noise. This method also has the advantage that it can utilize *a priori* information pertaining to bounds on epicardial potentials, potential gradients, or changes in geometry.

Solutions to the Forward and Problem of Electrocardiography using the Boundary Element Method

In this discussion, the forward and inverse problems of electrocardiography have been solved in terms of epicardial and body surface potentials. The method of the forward solution is the boundary element method applied to a realistic homogeneous human torso the result is a forward transfer coefficient matrix Z_{BH}. Direct inversion of Z_{BH} is not possible since the problem is ill-posed and any resulting inverse solution would be unstable. Therefore, we have applied the technique of regularization to compute a constrained inverse transfer coefficient matrix, Z_{HB}, with which epicardial potentials can be safely predicted from body surface potential maps. This section outlines the formulation of the problem and describes the steps involved in the generation of the forward solution matrix.

Analytical derivation

The starting point of the derivation is Green's second identity for two scalar, piecewise continuous functions, f and g, which states that

$$\int_S (f\nabla g - g\nabla f) \cdot d\vec{A} = \int_V (f\nabla^2 g - g\nabla^2 f)dV, \tag{1}$$

where, the Green's volume V is bounded by surface S whose outward directed element is denoted $d\vec{A}$. We can define the function f as $1/r$, where r is the distance from the source point q to an arbitrary field point p, called the *observation* point, and the function g as the scalar electric potential, ϕ. The area element, $d\vec{A}$ is defined as $\vec{n}\,dA$, where $\vec{n}$ is the outward normal to the surface and dA is the scalar element of area of the integrating surface. With these substitutions, the Green's identity now reads

$$\int_S (\frac{1}{r}\nabla\phi - \phi\nabla\frac{1}{r}) \cdot d\vec{A} = \int_V (\frac{1}{r}\nabla^2\phi - \phi\nabla^2\frac{1}{r})\,dV. \tag{2}$$

If there are no sources within the volume, V, the scalar potential ϕ satisfies the Laplace equation $\nabla^2\phi = 0$, and the first term of the volume integral disappears. The second term of the volume integral includes the expression $\nabla^2 r^{-1}$, which equals 0 for all $r \neq 0$. In the immediate vicinity of $r = 0$, ϕ can be considered constant so that the volume integral becomes

$$-\int_V \phi\nabla^2\frac{1}{r}\,dV = \phi(p_s)C, \tag{3}$$

where p_s represents the location of a singularity at which observation point and integration volume meet ($r = 0$) and

$$C = -\int_{V_s} \nabla^2\frac{1}{r}\,dV, \tag{4}$$

where V_s is the reduced volume which just includes the singularity. It can be shown [1] that in general the integrand may be written as

$$\nabla^2\frac{1}{r}\,dV = -4\pi\delta(\vec{r} - \vec{r'}), \tag{5}$$

where $\vec{r}$ and $\vec{r'}$ are vectors from the origin to the observation point and any point p within the volume of integration, respectively. The integral can now be evaluated as

$$-\int_{V_s} \nabla^2 \frac{1}{r} dV = \int_{V_s} 4\pi\delta(\vec{r} - \vec{r'})\, dV = \begin{cases} 0 & (p \text{ outside } V_s) \\ 4\pi & (p \text{ inside } V_s). \end{cases} \tag{6}$$

It is possible to choose an observation point anywhere within the Green's volume to satisfy equation 2. The standard approach is to select the observation point very close to the boundary of, but still within, the Green's volume. Physically, we can assume that the potential at such a point is virtually identical to that on the real surface in question, while mathematically, the points remain inside the volume and the result -4π can be used for the integral in equation 6. This approach was taken by both Barr *et al.* [2] and Messinger-Rapport and Rudy [3] and from equation 2 yields the following equation:

$$4\pi\phi(p) = \int_S (\frac{1}{r}\nabla\phi - \phi\nabla\frac{1}{r}) \cdot d\vec{A}. \tag{7}$$

A second strategy is possible, however, in which the observation point is located not just inside, but *on the surface*. It can be shown [4] that the integral in equation 3 can be evaluated at a point *on* the surface with the result -2π. This results in a slightly different form of equation 2 than that given in equation 7:

$$2\pi\phi(p) = \int_{S^-} (\frac{1}{r}\nabla\phi - \phi\nabla\frac{1}{r}) \cdot d\vec{A}, \tag{8}$$

the obvious difference being an additive factor of $2\pi\phi(p)$. S^- in this equation is the surface area excluding the singularity, that is, the integral is *proper-valued* and must be evaluated excluding the singularity at $r = 0$. To maintain consistency between the two equations 8 and 7, if the observation point is taken *close to but still inside* the surface of integration, then the volume integral of $\nabla^2(1/r)dV$ yields the result -4π, as in equation 6, and the surface integration is also performed over the *entire* surface; there is no singularity. If, on the other hand, the observation point is placed *on* the surface of integration, the volume integral yields the value -2π and the surface integral must be calculated by excluding the singularity, that is, as a proper-valued integral. Conceptually, placing the observation point on the surface is simpler and more accurate, and therefore, this approach is used in further discussion.

Figure 1 depicts the geometry to which we now apply Green's second identity. In this particular case, the Green's volume is the region enclosed by the epicardial and body surfaces, S_H and S_B, which together comprise S. We proceed from equation 8 by separating the surface which bounds the Green's volume V into the heart surface, S_H, and the body surface, S_B. The sense of the normal to the heart surface is redirected into the Green's volume so that by rearranging the integrals, we now have

$$2\pi\phi(p) = \int_{S_H} \phi\, d\Omega - \int_{S_B} \phi\, d\Omega - \int_{S_H} \frac{\nabla\phi}{r} \cdot d\vec{A} + \int_{S_B} \frac{\nabla\phi}{r} \cdot d\vec{A}. \tag{9}$$

We have introduced $d\Omega$, the incremental solid angle, for the $\nabla(1/r) \cdot d\vec{A}$ term and redirected the outward normal of the inner, epicardial surface to point into the Green's volume toward the body surface.

Equation 9 defines the potential at any point p on either part of the surface S (comprised of S_B and S_H), as a function of 1) the potential and normal component of potential-gradient on surface S_H and S_B, and 2) the location of the field point p relative to S_H and S_B. At the body-surface
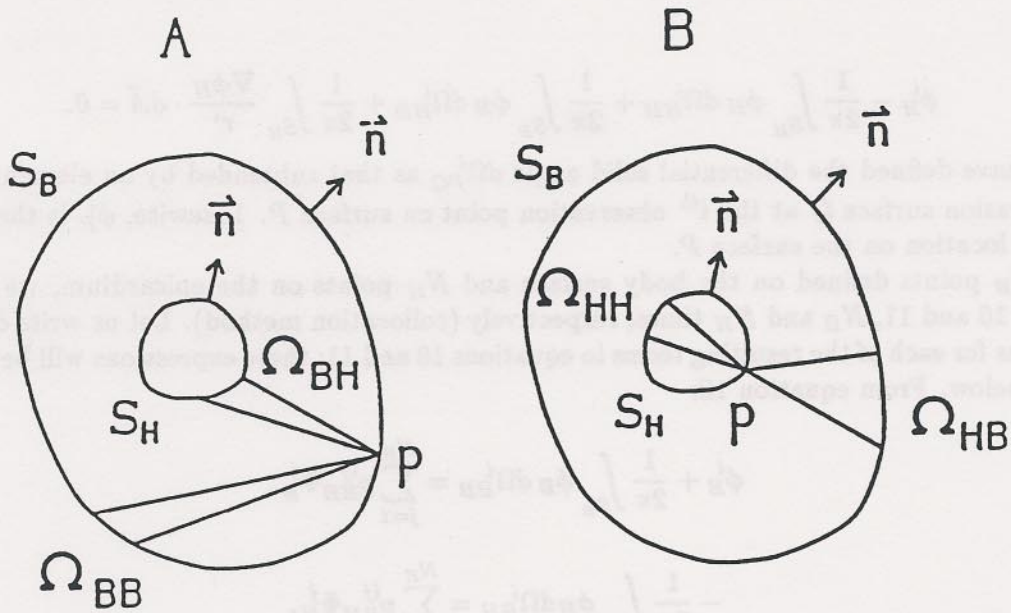
Figure 1: The geometry of the forward/inverse problem. In panel A, the observation point p is placed on the outer bounding body surface, S_B; in panel B, p lies on the inner bounding heart surface S_H. The Ω terms are the associated solid angles.

boundary S_B, the normal component of the potential gradient, $\nabla\phi_n = \nabla\phi \cdot d\vec{A}$, vanishes since the conductivity of the air is taken as zero, and hence the last term in equation 9 disappears. Since we are interested in deriving the relationship between potentials on S_H and S_B, we will place p first on one surface and then on the other and write equation 9 for each case. This situation is shown in Figure 1 for the case of an observation point on the body surface (panel A) and an observation point on the epicardial surface (panel B). The next section describes the development and solution of these equations.

Derivation of the coefficient matrices

The general approach to finding solutions to integral equations like equation 9 is to write one equation for each of a number of points on both of the surfaces and solve these equations simultaneously. This is known as the *collocation method* in numerical mathematics and provides a means of reducing an integration over an arbitrary smooth surface to a sum of (somewhat simpler) integrals, each of which can be evaluated separately [5]. The particular application of the collocation method to this problem originates with work of Barr, Ramsey and Spach [2] and their notation will be used throughout.

We start by rewriting equation 9 for two observation points placed on the body and epicardial surface, respectively, as

$$\phi_B^i - \frac{1}{2\pi}\int_{S_H}\phi_H\,d\Omega_{BH}^i + \frac{1}{2\pi}\int_{S_B}\phi_B\,d\Omega_{BB}^i + \frac{1}{2\pi}\int_{S_H}\frac{\nabla\phi_H}{r^i}\cdot d\vec{A} = 0 \qquad (10)$$

and

$$\phi_H^i - \frac{1}{2\pi} \int_{S_H} \phi_H \, d\Omega_{HH}^i + \frac{1}{2\pi} \int_{S_B} \phi_B \, d\Omega_{HB}^i + \frac{1}{2\pi} \int_{S_H} \frac{\nabla \phi_H}{r^i} \cdot d\vec{A} = 0. \tag{11}$$

Here we have defined the differential solid angle $d\Omega_{PQ}^i$ as that subtended by an elemental area of the integration surface Q at the ith observation point on surface P. Likewise, ϕ_P^i is the potential at the ith location on the surface P.

For N_B points defined on the body surface and N_H points on the epicardium, we can write equations 10 and 11, N_B and N_H times, respectively (collocation method). Let us write discretized expressions for each of the resulting terms in equations 10 and 11; these expressions will be examined in detail below. From equation 10:

$$\phi_B^i + \frac{1}{2\pi} \int_{S_B} \phi_B \, d\Omega_{BB}^i = \sum_{j=1}^{N_B} p_{BB}^{ij} \Phi_B^j, \tag{12}$$

$$-\frac{1}{2\pi} \int_{S_H} \phi_H d\Omega_{BH}^i = \sum_{j=1}^{N_H} p_{BH}^{ij} \Phi_H^j, \tag{13}$$

$$\frac{1}{2\pi} \int_{S_H} \frac{\nabla \phi_H}{r^i} \cdot d\vec{A}_H = \sum_{j=1}^{N_H} g_{BH}^{ij} \Gamma_H^j, \tag{14}$$

and from equation 11:

$$\frac{1}{2\pi} \int_{S_B} \phi_B \, d\Omega_{HB}^i = \sum_{j=1}^{N_B} p_{HB}^{ij} \Phi_B^j, \tag{15}$$

$$\phi_H^i - \frac{1}{2\pi} \int_{S_H} \phi_H d\Omega_{HH}^i = \sum_{j=1}^{N_H} p_{HH}^{ij} \Phi_H^j, \tag{16}$$

and

$$\frac{1}{2\pi} \int_{S_H} \frac{\nabla \phi_H}{r^i} \cdot d\vec{A}_H = \sum_{j=1}^{N_H} g_{HH}^{ij} \Gamma_H^j. \tag{17}$$

The argument of each of the summations can be separated into the product of a potential (Φ_B^j or Φ_H^j) or the gradient of a potential (Γ_H^j) at a specific point j on either one of the surfaces and a second factor (the $p's$ and $g's$) based entirely on the geometry of the torso and the heart. Φ_B^j and Φ_H^j are the potentials at node j on the body and heart surfaces, respectively; Γ_H^j is the normal component of the potential gradient for point j on the heart surface (the corresponding quantity is zero on the body surface). In general the g_{PQ}^{ij} term links the value of the potential gradient (Γ^j) at point j on surface P to the observation point i on surface Q while p_{PQ}^{ij} is the geometrical coefficient which weights the contribution of the potential at node j of surface Q to the potential at observation point i on surface P. The first subscript and superscript of each p or g term indicate the observation point, the second subscript and superscript, the element of the surface of integration; thus, for example, p_{HB}^{ij} is the coefficient for the observation point i on the epicardial surface and point j on the surface of integration, the body surface.

Now by inserting the appropriate right-hand sides of equations 12–17, we get the discretized equivalent equations to 10 and 11,

$$p^i_{BB}\Phi_B + p^i_{BH}\Phi_H + g^i_{BH}\Gamma_H = 0 \qquad (18)$$

and

$$p^i_{HB}\Phi_B + p^i_{HH}\Phi_H + g^i_{HH}\Gamma_H = 0, \qquad (19)$$

where the summations over j are implicit in each term and i refers to a specific observation point on either the heart (equation 19) or the body (equation 18) surface. The p and g terms are the row vectors which express the geometrical contribution of each point on the surface of integration to the potential at the observation point i. If we write equation 18 for each point on the body surface and equation 19 for each point on the heart surface, two sets of equations result, which in matrix notation can be written as:

$$P_{BB}\Phi_B + P_{BH}\Phi_H + G_{BH}\Gamma_H = 0 \qquad (20)$$

and

$$P_{HB}\Phi_B + P_{HH}\Phi_H + G_{HH}\Gamma_H = 0. \qquad (21)$$

The $P's$ and $G's$ are the matrices formed by collocating all the elements of the associated p^i and g^i row vectors, one row for each observation point. For the P_{HB} matrix, for example, each row contains N_H elements from one p^i_{HB} vector, and there are N_H rows, each representing a different value of i. Here again, the first subscript represents the surface containing the observation points, the second subscript the surface of integration. P_{HH} and G_{HH} are square matrices of size $N_H \times N_H$, P_{BH} and G_{BH} are sized $N_B \times N_H$, P_{BB} is another square matrix of size $N_B \times N_B$, and P_{HB} is sized $N_H \times N_B$.

By solving the equation 21 for Γ_H and substituting the result into equation 20 we remove the need for explicit knowledge of the potential gradients. This leads, after sorting of variables, to

$$(P_{BB} - G_{BH}G^{-1}_{HH}P_{HB})\Phi_B = (G_{BH}G^{-1}_{HH}P_{HH} - P_{BH})\Phi_H, \qquad (22)$$

which can be rewritten as

$$\Phi_B = Z_{BH}\Phi_H, \qquad (23)$$

with Z_{BH} defined as

$$Z_{BH} = (P_{BB} - G_{BH}G^{-1}_{HH}P_{HB})^{-1}(G_{BH}G^{-1}_{HH}P_{HH} - P_{BH}). \qquad (24)$$

Equations 23 and 24 define the solution to the forward problem in the desired form; Z_{BH} is the transfer coefficient matrix which directly relates epicardial potentials to body surface potentials. It remains to examine each term of equation 22 and develop accurate computational methods for evaluating the elements of all the matrices involved. Once this has been achieved, we may convert epicardial potentials into body surface potentials and, thus, solve the forward problem.

References

[1] J.D. Jackson. *Classical Electrodynamics*. John Wiley & Sons, New York, 1975. Second edition.

[2] R.C. Barr, M. Ramsey, and M.S. Spach. Relating epicardial to body surface potential distributions by means of transfer coefficients based on geometry measurements. *IEEE Trans. Biomed. Eng.*, BME-24:1–11, 1977.

[3] B.J. Messinger-Rapport and Y. Rudy. Regularization of the inverse problem in electrocardiography: a model study. *Math. Biosci.*, 89:79–118, 1988.

[4] A.C.L. Barnard, I.M. Duck, and M.S. Lynn. The application of electromagnetic theory to electrocardiology: I Derivation of the integral equation. *Biophys. J*, 7:443–462, 1967.

[5] C.W. Steele. *Numerical Computation of Electrical and Magnetic Fields*. Van Nostrand Reinhold, New York, 1987.